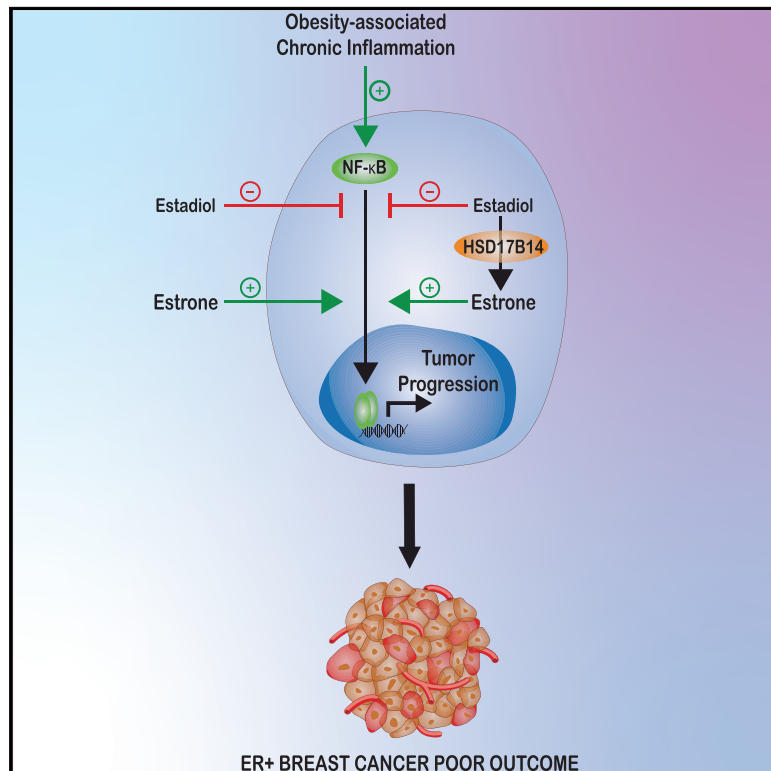


Cell Metabolism

The Major Pre- and Postmenopausal Estrogens Play Opposing Roles in Obesity-Driven Mammary Inflammation and Breast Cancer Development

Graphical Abstract



Authors

Rehana Qureshi, Manuel Picon-Ruiz, Iskander Aurrekoetxea-Rodriguez, ..., Susan Kesmodel, Maria del Mar Vivanco, Joyce M. Slingerland

Correspondence

rxq58@med.miami.edu (R.Q.), mpicon@ugr.es (M.P.-R.), jslingerland@med.miami.edu (J.M.S.)

In Brief

Slingerland and colleagues show that the major premenopausal estrogen, 17β-estradiol, and postmenopausal estrone play opposing roles to inhibit or drive, respectively, the tumor-promoting effects of inflammation and obesity. Estrone is pro-inflammatory and pro-oncogenic. It increases with obesity and stimulates expansion of stem-like cells in hormone-sensitive breast cancer to drive rapid tumor growth.

Highlights

- Menopause, obesity, and cancer increase pro-inflammatory cytokines in human breast fat
- Estrone stimulates and estradiol relieves the inflammation of obesity *in vivo*
- Estrone cooperates with NFκB to induce inflammatory mediators, but estradiol does not
- *HSD17B14* increases intracellular estrone to drive inflammation and ER+ CSC expansion



Article

The Major Pre- and Postmenopausal Estrogens Play Opposing Roles in Obesity-Driven Mammary Inflammation and Breast Cancer Development

Rehana Qureshi,^{1,12,*} Manuel Picon-Ruiz,^{1,2,3,12,*} Iskander Aurrekoetxea-Rodriguez,^{1,4} Vanessa Nunes de Paiva,¹ Massimo D'Amico,¹ Hyunho Yoon,¹ Ramya Radhakrishnan,¹ Cynthia Morata-Tarifa,¹ Tan Ince,⁵ Marc E. Lippman,⁶ Seth R. Thaller,⁷ Steven E. Rodgers,^{1,8} Susan Kesmodel,^{1,8} Maria del Mar Vivanco,⁴ and Joyce M. Slingerland^{1,9,10,11,13,*}

¹Braman Family Breast Cancer Institute, Sylvester Comprehensive Cancer Center, Miami, FL 33136, USA

²Department of Human Anatomy and Embryology, Faculty of Medicine, Biopathology and Medicine Regenerative Institute (IBIMER), and Excellence Research Unit "Modeling Nature" (MNat), University of Granada, Granada, Spain

³Biosanitary Institute of Granada (ibs.GRANADA), Granada, Spain

⁴Center for Cooperative Research in Biosciences (CIC bioGUNE), Basque Research and Technology Alliance (BRTA), Bizkaia Technology Park, 48160 Derio, Spain

⁵Department of Pathology, Weill Cornell Medicine and New York Presbyterian Brooklyn Methodist Hospital, New York, NY, USA

⁶Breast Cancer Program, Lombardi Comprehensive Cancer Center, Department of Oncology, Georgetown University, Washington, D.C., USA

⁷Department of Plastic Surgery, Miller School of Medicine, University of Miami, Miami, FL, USA

⁸Division of Surgical Oncology, Department of Surgery, Miller School of Medicine, University of Miami, Miami, FL, USA

⁹Department of Medicine, Miller School of Medicine, University of Miami, Miami, FL, USA

¹⁰Department of Biochemistry and Molecular Biology, Miller School of Medicine, University of Miami, Miami, FL, USA

¹¹Present address: Breast Cancer Program, Lombardi Comprehensive Cancer Center, Department of Oncology, Georgetown University, Washington, D.C., USA

¹²These authors contributed equally

¹³Lead Contact

*Correspondence: rxq58@med.miami.edu (R.Q.), mpicon@ugr.es (M.P.-R.), jslingerland@med.miami.edu (J.M.S.)

<https://doi.org/10.1016/j.cmet.2020.05.008>

SUMMARY

Many inflammation-associated diseases, including cancers, increase in women after menopause and with obesity. In contrast to anti-inflammatory actions of 17 β -estradiol, we find estrone, which dominates after menopause, is pro-inflammatory. In human mammary adipocytes, cytokine expression increases with obesity, menopause, and cancer. Adipocyte:cancer cell interaction stimulates estrone- and NF κ B-dependent pro-inflammatory cytokine upregulation. Estrone- and 17 β -estradiol-driven transcriptomes differ. Estrone:ER α stimulates NF κ B-mediated cytokine gene induction; 17 β -estradiol opposes this. In obese mice, estrone increases and 17 β -estradiol relieves inflammation. Estrone drives more rapid ER $^{+}$ breast cancer growth *in vivo*. HSD17B14, which converts 17 β -estradiol to estrone, associates with poor ER $^{+}$ breast cancer outcome. Estrone and HSD17B14 upregulate inflammation, ALDH1 activity, and tumorspheres, while 17 β -estradiol and HSD17B14 knockdown oppose these. Finally, a high intratumor estrone:17 β -estradiol ratio increases tumor-initiating stem cells and ER $^{+}$ cancer growth *in vivo*. These findings help explain why postmenopausal ER $^{+}$ breast cancer increases with obesity, and offer new strategies for prevention and therapy.

Context and Significance

Estrogen receptor-positive (ER $^{+}$) breast cancer risk increases with obesity after menopause, but not before. A new clue to this paradox lies in the opposing actions of pre- and postmenopausal estrogens on inflammation. After menopause, 17 β -estradiol production falls and estrone dominates. Here, researchers from the University of Miami and their colleagues show that while premenopausal 17 β -estradiol is anti-inflammatory, estrone promotes inflammation in diet-induced obesity. Estrone activates pro-inflammatory genes associated with poor ER $^{+}$ breast cancer outcome. A high estrone:17 β -estradiol ratio, as exists after menopause and increases with obesity, drives inflammation and stimulates hormone-sensitive breast cancer initiation and tumor growth. This work sheds new light on the increase in inflammatory diseases, including cancer, in women after menopause.



INTRODUCTION

Recent decades have seen an alarming rise in the prevalence of obesity worldwide. It has been estimated that by 2030, up to 51% of the population will be obese (Finkelstein et al., 2012; Ward et al., 2019). In addition to known associations with heart disease and diabetes, obesity is associated with increased risk and worse outcome for several cancers, including breast cancer (Renehan et al., 2015). Breast cancer is the most common cancer and second leading cause of cancer death in women worldwide, and risk rises progressively after menopause (Ferlay et al., 2015). Over 60% of breast cancers are estrogen receptor-positive (ER+) (Howlader et al., 2014; Lippman, 1976) and a majority of these arise after menopause. The risk of postmenopausal ER+ breast cancer increases nearly 40% with obesity (Munsell et al., 2014; Picon-Ruiz et al., 2017; Suzuki et al., 2009). Regardless of age at diagnosis and disease subtype, breast cancer mortality is increased by over 2-fold with obesity (Calle et al., 2003; Chan et al., 2014; Picon-Ruiz et al., 2017). Thus, the rise in breast cancer mortality worldwide in the last few decades may reflect, in part, the increased prevalence of obesity (Wang et al., 2015). Given the rapid rise of obesity, its impact on breast and other cancers may not be fully appreciated.

Interestingly, the relationship between obesity and ER+ breast cancer risk differs before and after menopause. Before menopause, obese women have a 10% reduction in ER+ breast cancer risk, as compared to the 40% increased risk with obesity thereafter (Renehan et al., 2015). These differences in obesity-associated breast cancer risk might be linked to hormonal differences before and after menopause. After menopause, the principal estrogen of reproductive years, ovarian 17 β -estradiol (E2), is markedly decreased and estrone (E1) becomes the main estrogen in tissue and circulation. E1 is produced through conversion of adrenal androstenedione by aromatase, largely in adipose, breast, bone, and brain tissue (Grodin et al., 1973; Nimrod and Ryan, 1975; Santen et al., 2009; Siiteri, 1982; Siiteri and MacDonald, 1973). Adipose tissue is the major component of the postmenopausal breast. Androstenedione conversion to E1 increases by nearly 2-fold in obesity, not due to increased androstenedione production (Siiteri and MacDonald, 1973), but due to its increased aromatization in the expanded obese adipose tissue (Nimrod and Ryan, 1975; Schindler et al., 1972). Serum E2 and E1 levels are over 2-fold higher in obese compared to lean postmenopausal women (Key et al., 2002, 2003, 2015), and epidemiologic multivariate analyses indicate that estrogens are the most important factors associated with the excess breast cancer risk with obesity (Key et al., 2015). Some studies suggest that the association between postmenopausal ER+ breast cancer risk and serum E1 is greater than that for E2 (Adly et al., 2006; Miyoshi et al., 2003; Vincze et al., 2015; Yu et al., 2003). While estrogen levels in serum are not, per se, breast cancer drivers, they are more readily measured than those in mammary tissue and reflect changes in estrogens in the breast, in fat, and in mammary adipose stroma that are.

Obese adipose tissue is a site of chronic inflammation and acts as an endocrine organ, releasing bioactive adipokines, cytokines, chemokines, and hormone-like factors (Hoy et al., 2017; Picon-Ruiz et al., 2017; Quail and Dannenberg, 2019). In

obesity, adipocytes produce less of the pro-differentiation hormone, adiponectin, and more of the pre-adipocyte mitogen, leptin. The expanded pre-adipocyte population produces pro-inflammatory/angiogenic cytokines, including interleukin 6 (IL6), IL8, chemokine (C-C motif) ligand 2 (CCL2), CCL5, and vascular endothelial growth factor A (VEGFA), to drive pre-adipocyte proliferation and vasculogenesis. These recruit macrophages and T lymphocytes, inducing a chronic inflammatory state (Picon-Ruiz et al., 2017; Vona-Davis and Rose, 2009).

Obese adipose tissue inflammation is activated and maintained by the NF κ B pathway in adipocytes and invading immune cells through their Toll-like receptors (Barton, 2008; Hotamisligil and Erbay, 2008; Medzhitov, 2008). High concentrations of inflammatory cytokines induce adipocyte lipolysis, releasing free fatty acids (Tornatore et al., 2012) that stimulate adipocyte TLR4 to activate NF κ B (Schäffler and Schölmerich, 2010). The NF κ B family comprises homo- and heterodimers of RelA, c-Rel, RelB, NF κ B1 (p105/p50), and NF κ B2 (p100/p55) transcription factors that modulate gene expression in response to infection, inflammation, hypoxia, and cytokines (Vallabhapurapu and Karin, 2009). These are sequestered in the cytoplasm by I κ Bs, whose phosphorylation by I κ B kinases (IKK α , β , and γ) permits nuclear translocation of NF κ B factors to activate gene expression. NF κ B targets encode inflammatory mediators, including tumor necrosis factor- α (TNF α), IL-1 β , and cytokines that feed forward to maintain inflammation (Vallabhapurapu and Karin, 2009). The NF κ B pathway not only drives obesity-mediated inflammation, but its constitutive activation in many cancers promotes proliferation, angiogenesis, and metastasis (Grivennikov et al., 2010).

The interaction between estrogen and NF κ B signaling is complex. E2-bound ER α plays a well-established anti-inflammatory role, opposing NF κ B in several diseases, including inflammatory bowel disease, multiple sclerosis, and arthritis (Kalaitzidis and Gilmore, 2005). E2-bound ER α inhibits NF κ B action via induction of the I κ B gene, and through non-genomic crosstalk that decreases IKK activation and impairs nuclear p65 localization (Frasor et al., 2015; Kalaitzidis and Gilmore, 2005). While E2-bound ER α localizes to genomic estrogen response elements (EREs) to modulate target gene expression, upon TNF α -stimulated NF κ B activation, ER α shifts from predominantly EREs to occupy NF κ B response elements (κ BREs) and alters RelA/p65 target gene induction (Franco et al., 2015; Kalaitzidis and Gilmore, 2005). E2/ER α binds κ BRE sites in the CCL2 and/or IL6 promoters to inhibit their induction in astrocytes (Giraud et al., 2010), breast cancer (Nettles et al., 2008), and immune cells (Ghisletti et al., 2005). Although E2 has well-described anti-inflammatory actions, how the NF κ B pathway interacts with E1, the dominant estrogen after menopause, is not well described.

We recently showed that interaction between breast cancer cells and immature adipocytes upregulates cytokines IL6, IL8, CCL5, and CCL2, and activates Src to increase cancer stem-like cells, tumor initiation, and metastasis (Picon-Ruiz et al., 2016). While both cell types upregulated inflammatory cytokines, production by adipocytes was considerably greater than that of the cancer cells; thus, cancer-associated adipocytes may be major drivers of inflammation. Each cytokine contributed to cancer stem cell (CSC) expansion, which would facilitate tumor progression following local invasion into breast fat (Picon-Ruiz

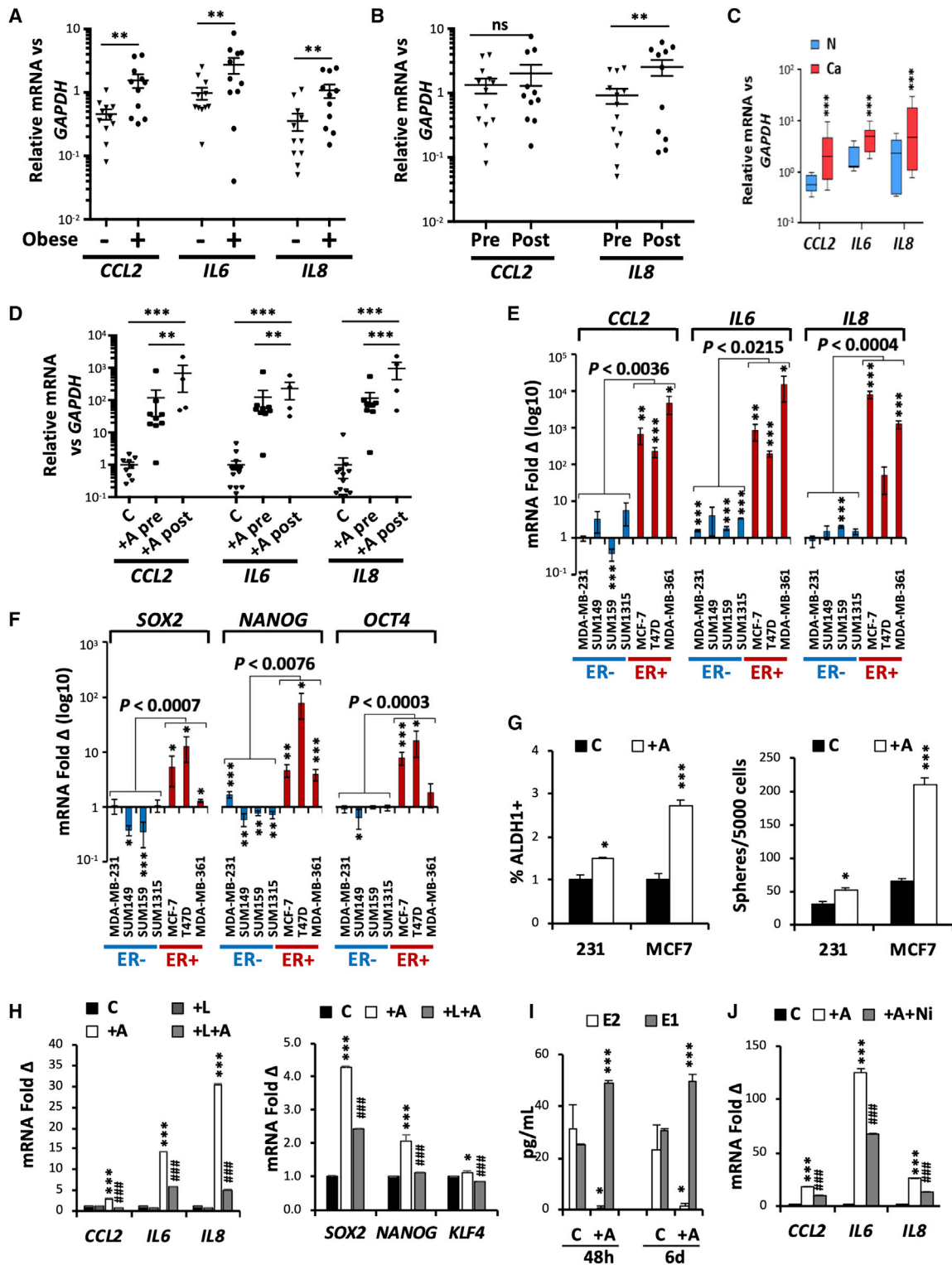


Figure 1. Inflammatory Cytokines Increase with Obesity, Menopause, and Cancer in Human Mammary Adipocytes and Are Induced via E1 and NFκB upon Adipocyte:Cancer Cell Interaction

(A and B) Cytokines assayed by qPCR in breast adipocytes from non-obese (n = 11) and obese (n = 11) premenopausal women (A), and from premenopausal (n = 13) and postmenopausal (n = 11) obese women (B) graphed relative to GAPDH (**p < 0.01).

(C) qPCR of adipocytes cytokines in peritumoral (Ca) or contralateral unaffected “normal” (N) breast fat from four patients undergoing bilateral mastectomy for unilateral breast cancer (****p < 0.001).

(legend continued on next page)

et al., 2016). The present work investigated how the dominant estrogens before and after menopause interact with NF κ B to affect inflammation and breast cancer development.

It is paradoxical that ER+ breast cancer increases after menopause and that the excess risk of ER+ breast cancer with obesity is limited to the postmenopausal period, when total estrogen levels decrease. Here, we investigated the hypothesis that the dominant postmenopausal estrogen, E1, might have an opposite effect to E2, and activate NF κ B-mediated inflammation to promote ER+ tumor emergence after menopause. Present data indicate that, in contrast to E2, which has anti-inflammatory effects, E1 cooperates with NF κ B to mediate inflammation. E1 increases inflammation accompanying high-fat diet (HFD)-induced obesity *in vivo*, while E2 opposes it. In the context of TNF α activation, E1 and E2 stimulate different global gene expression patterns, with E1 further upregulating genes of poor prognostic significance in ER+ breast cancer. While E2 opposes coactivator CBP recruitment to κ B sites on cytokine gene promoters, E1 stimulates its recruitment and chromatin H3K27 acetylation to drive cytokine expression and increase CSCs and tumorigenesis. Present work may help explain the rise in ER+ breast cancer incidence after menopause and inform the pathophysiology of chronic inflammation-related diseases of higher male prevalence that increase after menopause in women.

RESULTS

Inflammatory Cytokines in Mammary Adipocytes Increase with Obesity, Menopause, and Cancer

While obese adipose tissue is a site of chronic inflammation (Toratoure et al., 2012), how estrogens regulate production of inflammatory mediators in mammary fat is not fully characterized. Circulating E2, of ovarian origin, falls from 30–500 pg/mL before to <10 pg/mL after menopause. In contrast, pre- and postmenopausal serum E1 levels are similar (25–30 pg/mL), but more than double in obese women to 60–80 pg/mL (Eliassen et al., 2006; Kaaks et al., 2005; Key et al., 2015), due to increased synthesis by aromatase in fat tissue and in the breast. Levels of both estrogens in the postmenopausal breast are higher than in serum and at similar concentrations (close to 80–110 pg/mL or 0.4–0.6 nM) in the postmenopausal breast (Bonney et al., 1983; Lønning et al., 2011; van Landeghem et al., 1985). Since adipocytes are a major site of both E1 (Siiteri and MacDonald, 1973) and pro-inflammatory cytokine production (Picon-Ruiz et al., 2016), we assayed cytokine secretion from mature human adipocytes from fat tissues. Of over 45 cytokines assayed, CCL2, IL6, and IL8 were most abundant (Figures S1A and S1B). Their expres-

sion was then compared in mammary adipocytes from women of different body weight and menopausal status. Expression of CCL2, IL6, and IL8 was higher in mammary adipocytes from obese (n = 11) than from non-obese premenopausal women (n = 11; Figure 1A). Postmenopausal obese donors had higher mammary adipocyte CCL2 and IL8 expression than obese premenopausal donors (trend to significance for CCL2, p < 0.01 for IL8; Figure 1B). In women undergoing bilateral mastectomy for breast cancer, peritumoral breast fat expressed higher levels of CCL2, IL6, and IL8 than adipocytes from the contralateral unaffected breast (Figure 1C). Thus, mammary adipocyte inflammation appears to increase with obesity, when ovarian E2 falls after menopause and in cancer-associated breast tissue.

Cytokine Induction upon Adipocyte: Cancer Cell Contact Is Stimulated by Estrone and NF κ B

Breast cancer cells invading beyond ductal basement membranes encounter peritumoral adipocytes, the most abundant mammary stromal component. We previously showed breast cancer cell interaction with adipocytes stimulates pro-inflammatory cytokine production (Picon-Ruiz et al., 2016). Here, we evaluated how estrogens affect this cytokine upregulation. Mammary adipocytes from obese postmenopausal women not only expressed higher CCL2 and IL8 than those from premenopausal donors (Figure 1B), but they also stimulated greater cytokine induction by MCF7 ER+ breast cancer cells following co-culture (Figure 1D). Furthermore, co-culture of mature adipocytes with ER+ or ER- breast cancer cells showed CCL2, IL6, and IL8 induction was greater in ER+ than in ER- breast cancer lines (Figures 1E and S1C). Both findings suggest a role for estrogen:ER α in cytokine induction. Similarly, SOX2, NANOG, and OCT4 expression (Figures 1F and S1D), and enrichment of ALDH1+ and mammosphere-forming cells (features of stem-like cancer cells), were greater in ER+ than ER- breast cancer cells following co-culture with mature adipocytes (Figures 1G, S1E, and S1F).

As noted earlier, mature adipose tissue is a major site of E1 production by aromatase (Nimrod and Ryan, 1975; Schindler et al., 1972; Siiteri, 1982; Siiteri and MacDonald, 1973). To test further if estrogens regulate cytokine induction during co-culture, MCF7 co-cultures with mature mammary adipocytes from 3 independent donors were treated with the aromatase inhibitor letrozole (Santen et al., 2009). Inhibition of estrogen production by letrozole impaired cytokine and embryonic stem cell-transcription factor (ESC-TF) gene induction in MCF7 cells following co-culture (Figures 1H, S1G, and S1H). Notably, while fresh culture medium has similar E1 and E2 concentrations

(D) Cytokine expression in MCF7 alone (control, C), or co-cultured 6 days with breast adipocytes from premenopausal (n = 9, +A pre) or postmenopausal (n = 4, +A post) obese women graphed versus GAPDH (**p < 0.01, ***p < 0.001).

(E and F) Cytokine (E) and ESC-TF expression (F) in ER- and ER+ breast cancer lines \pm co-culture with mature adipocytes for 6 days, normalized to 1 for monocultures (C) (n = 9; *p < 0.05, **p < 0.01, ***p < 0.001).

(G) Mean ALDH1 fluorescence (left) and mammosphere/cells (right) seeded in MCF7 after 6 days of culture alone (C) or with adipocytes (+A) (n = 3; *p < 0.05, ***p < 0.001).

(H) qPCR of cytokine (left) and ESC-TF expression (right) in MCF7 monoculture (C) and after 6 day co-culture with mammary adipocytes (+A) or with 10 nM letrozole (+A+L), normalized as above (n = 3; *p < 0.05, ***p < 0.001 versus C; ###p < 0.001 versus +A).

(I) Estradiol (E2) and estrone (E1) in supernatant from MCF7 monoculture (C) or with adipocytes (+A) for 48 h and 6 days (n = 3; *p < 0.05, **p < 0.01 versus C).

(J) Cytokines in MCF7 co-cultured for 6 days with adipocytes (+A) or with addition of NF κ B inhibitor, 1 μ M BAY 11-7082 (+A+Ni), normalized as above (n = 3; ***p < 0.001 versus C; ###p < 0.001 versus +A).

All graphed data show mean \pm SEM. See also Figure S1.

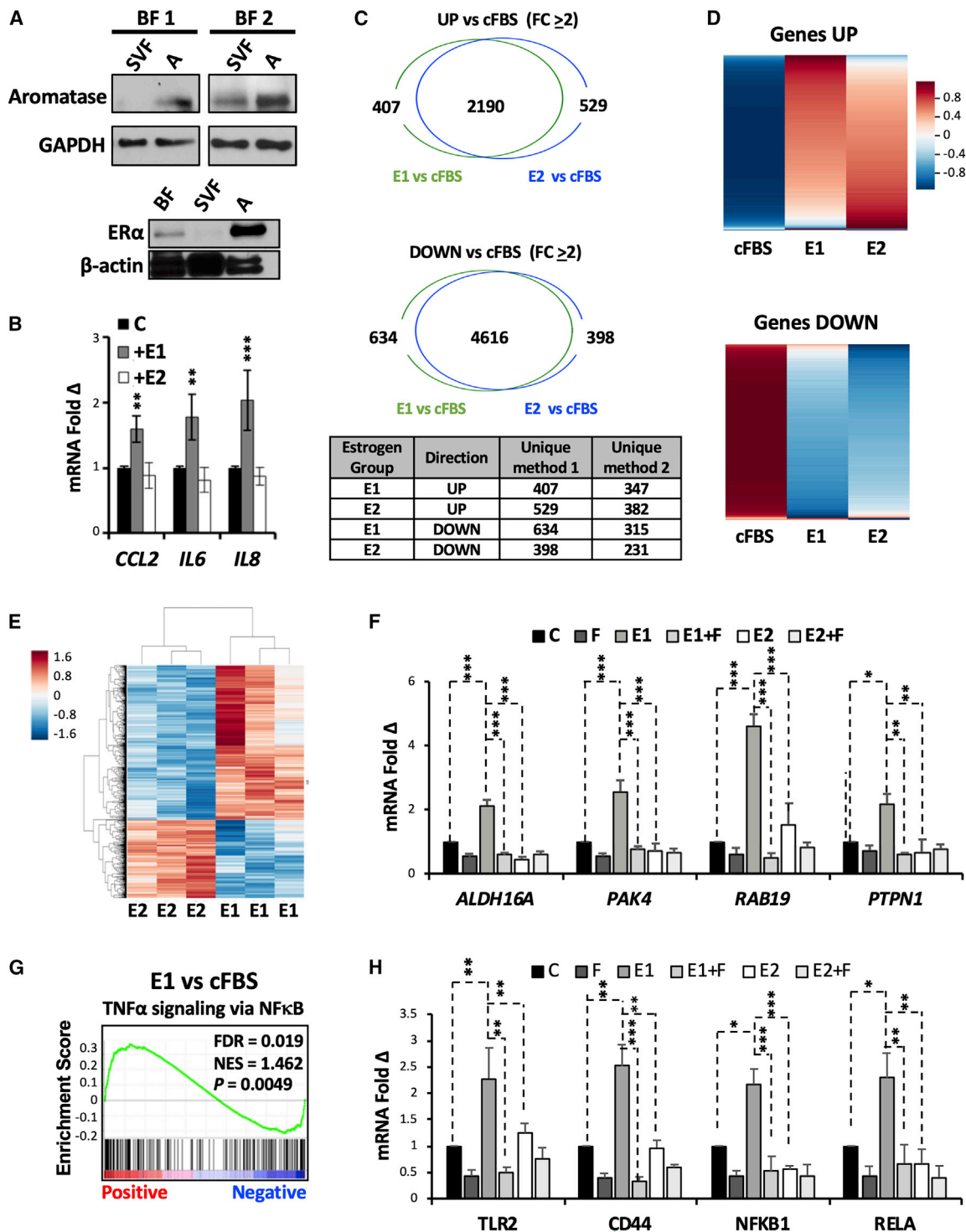


Figure 2. Estrone- and 17 β -Estradiol-Driven Transcriptomes Are Not Identical

(A) Western blot of aromatase from mammary tissue stromal vascular fraction (SVF) and mammary adipocytes (A), with GAPDH loading control (top), and of ER α from breast fat tissue (BF), SVF, and adipocytes (A) with β -actin loading control (bottom).

(B) Cytokine expression in mammary adipocytes treated 2 h with DMSO vehicle (C), or 10 nM E1 or E2 (mean \pm SEM graphed normalized to 1 for vehicle control, C; n = 3; **p < 0.01, ***p < 0.001).

(C–F) Estrogen-starved MCF7 (cFBS) were treated with DMSO vehicle alone, 10 nM E1, or 10 nM E2 for 8 h followed by sample recovery for RNA-seq. All RNA-seq analyses were based on 3 biologic repeat assays. Venn diagrams of genes up- (top) or downregulated (bottom) by ≥ 2 -fold (FC ≥ 2 , q < 0.05). Table shows numbers of uniquely up- or downregulated genes from the Venn diagram (method 1) that were retained using a second method of analysis (method 2, q < 0.05).

(legend continued on next page)

(reflecting near-equal concentrations in fetal bovine serum, FBS), E2 levels fell within 48 h of co-culture and E1 became the dominant estrogen, persisting over the next 6 days (Figure 1I). Thus, cytokine induction and the consequent increase in stem-like cells following breast cancer cell:adipocyte co-culture are E1 dependent.

Since NF κ B critically regulates inflammation (Vallabhapurapu and Karin, 2009), we assayed its role in co-culture-mediated cytokine induction. Adipocyte co-culture with MCF7 shifted p65/RelA from cytoplasm to nucleus and upregulated NF κ B luciferase activity within 24 h in MCF7 cells (Figures S1I and S1J). NF κ B inhibition using either of two different drug inhibitors, BAY11-78082 (Ling and Kumar, 2012) or TCPA-1, during co-culture attenuated *IL6*, *IL8*, and *CCL2* induction in MCF7 (Figures 1J and S1K, respectively). Thus, cytokine induction following cancer cell contact with adipocytes is stimulated by both E1 and NF κ B activation.

Estrone- and Estradiol-Driven Transcriptomes Are Not Identical

Since E2 is known to oppose cytokine gene induction by NF κ B (Giraud et al., 2010; Kalaitzidis and Gilmore, 2005; Nettles et al., 2008) and since E1 promoted *CCL2*, *IL6*, and *IL8* induction in our co-culture assays, we next tested if pre- and postmenopausal estrogens might have different effects on inflammatory and overall gene expression profiles. In mammary adipose tissue, aromatase and ER α levels are greater in mature adipocytes than in the stromal vascular fraction (SVF) (Figure 2A). Surprisingly, in both mature adipocytes and in MCF7, E1 did not function as a slightly weaker but identical agonist to E2. Rather, these estrogens had different actions. In isolated mammary adipocytes, E1 upregulated *CCL2*, *IL6*, and *IL8* expression within 2 h while E2 did not (Figure 2B).

Global gene expression patterns stimulated by each hormone were next assayed. ER $^+$ breast cancer cell lines are grown in 10 nM E2 (Engel et al., 1978; Lippman et al., 1976; Strobl and Lippman, 1979) because at this dose, proliferation and protein synthesis are maximal and E2 saturates ER α in cultured ER $^+$ cancer lines. Effects of E1 on protein synthesis and receptor binding are also maximal at 10 nM (Lippman et al., 1976, 1977; Sasson and Notides, 1983); thus, we used 10 nM for these assays. Global gene responses to E1 and E2 differed: at 8 h after addition of each steroid versus DMSO control to estrogen-starved MCF7, nearly 20% of E1-upregulated genes and 12% of E1-downregulated genes were not affected by E2 (fold change versus cFBS, FC \geq 2-fold and $q < 0.05$; Figure 2C, top). Uniquely E1 and E2 upregulated genes are listed in Tables S1 and S2. All RNA sequencing (RNA-seq) experiments were performed in triplicate in independent biologic repeat assays. Differential expression was further evaluated in a second analysis in which all E1

and E2 data were combined and then compared against the cFBS group. Numbers of uniquely up- or downregulated genes shown in the Venn diagram are shown as “unique, method 1” in Figure 2C. The “unique, method 2” column shows those genes uniquely up- or downregulated by the indicated steroid in method 1 (from Venn diagram) that remain differentially expressed even when E1 and E2 samples are combined before comparison (method 2, $q < 0.05$). Most uniquely regulated genes from method 1 remained significant using the second analysis method. Perhaps more importantly, those estrogen-regulated genes that were commonly up- or downregulated by both estrogens differed considerably in their extent of change (any FC, $q < 0.05$; Figure 2D). The heatmap of a subset of genes differentially expressed 8 h after ligand addition is shown in Figure 2E.

Gene induction following addition of E1, but not E2, was verified by qPCR in a selection of genes (Figure 2F). Selected genes that were uniquely E2 induced from Figure 2C were also validated by qPCR (Figure S2A). E1 and E2 actions were both inhibited by prior addition 10 nM of the drug fulvestrant (ICI182,780), which blocks the ER and mediates its degradation. When compared to estrogen-starved (cFBS) cells, gene ontology (GO) analysis showed E1 and E2 activate many common pathways, but only E1 stimulated NF κ B activation in MCF7 (Figure 2G). Upregulation of a selection of these NF κ B pathway genes by E1, but not E2, was also verified by qPCR and was inhibited by 10 nM fulvestrant (Figure 2H). Thus, we make the unprecedented observation that effects of E1 and E2 on gene expression differ importantly, with E1 alone mediating inflammatory NF κ B pathway activation.

Estrone Cooperates with NF κ B to Induce Inflammatory Mediators in ER $^+$ Breast Cancer Lines

Since genomic profiling showed E1 drives NF κ B activation, we next compared E1 and E2 effects on NF κ B activity in MCF7. Since estrogen-deprived MCF7 have little basal NF κ B activity, estrogens were added over a range of concentrations 30 min after TNF α (10 ng/mL). Notably, in estrogen-deprived MCF7, E2 decreased NF κ B luciferase activation by TNF α in an ER-dependent manner (Figure 3A), consistent with its known anti-inflammatory effect, but E1 did not. E2 (10 nM), added 30 min after TNF α (10 ng/mL), opposed *CCL2* and *IL6* induction, while E1 further stimulated TNF α -mediated cytokine gene induction in both MCF7 and a second ER $^+$ breast cancer line, MDA-MB-361 (Figures 3B and S2B). Both TNF α +E1 and TNF α +E2 effects on *CCL2* and *IL6* were opposed by prior ER blockade by 10 nM fulvestrant (Figure 3B). Fulvestrant alone did not affect cytokine expression in estrogen-deprived MCF7.

E1 and E2 effects on ER α and NF κ B assembly were compared at a well-characterized κ B site $-2,600$ bp from the *CCL2* start site (Giraud et al., 2010) using chromatin immunoprecipitation

(C) Heatmaps show different extents of gene up- (top) or downregulation (bottom) ($q < 0.05$) in triplicate repeat RNA-seq samples.

(D) Heatmap showing genes differentially regulated in E1 versus E2 treated MCF7.

(E) qPCR validation of genes specifically upregulated by E1 (from Table S1).

(F) Estrogen-starved MCF7 (cFBS) were treated with DMSO vehicle (C), 10 nM E1, or 10 nM E2 \pm 10 nM fulvestrant (F) 8 h and then indicated genes assayed by qPCR and graphed as mean \pm SEM ratio of expression versus GAPDH and normalized to 1 for vehicle controls (C) ($n = 3$; * $p < 0.05$, ** $p < 0.01$, *** $p < 0.001$).

(G) GSEA of TNF α signaling activation by E1 versus cFBS (NES, normalized enrichment score; FDR, false discovery rate).

(H) The same cells recovered in part (F) above were used for qPCR validation of TNF α /NF κ B pathway genes specifically upregulated by E1.

All graphed data show mean \pm SEM. Where error bars are not evident, the SEM was very small. See also Figure S2.

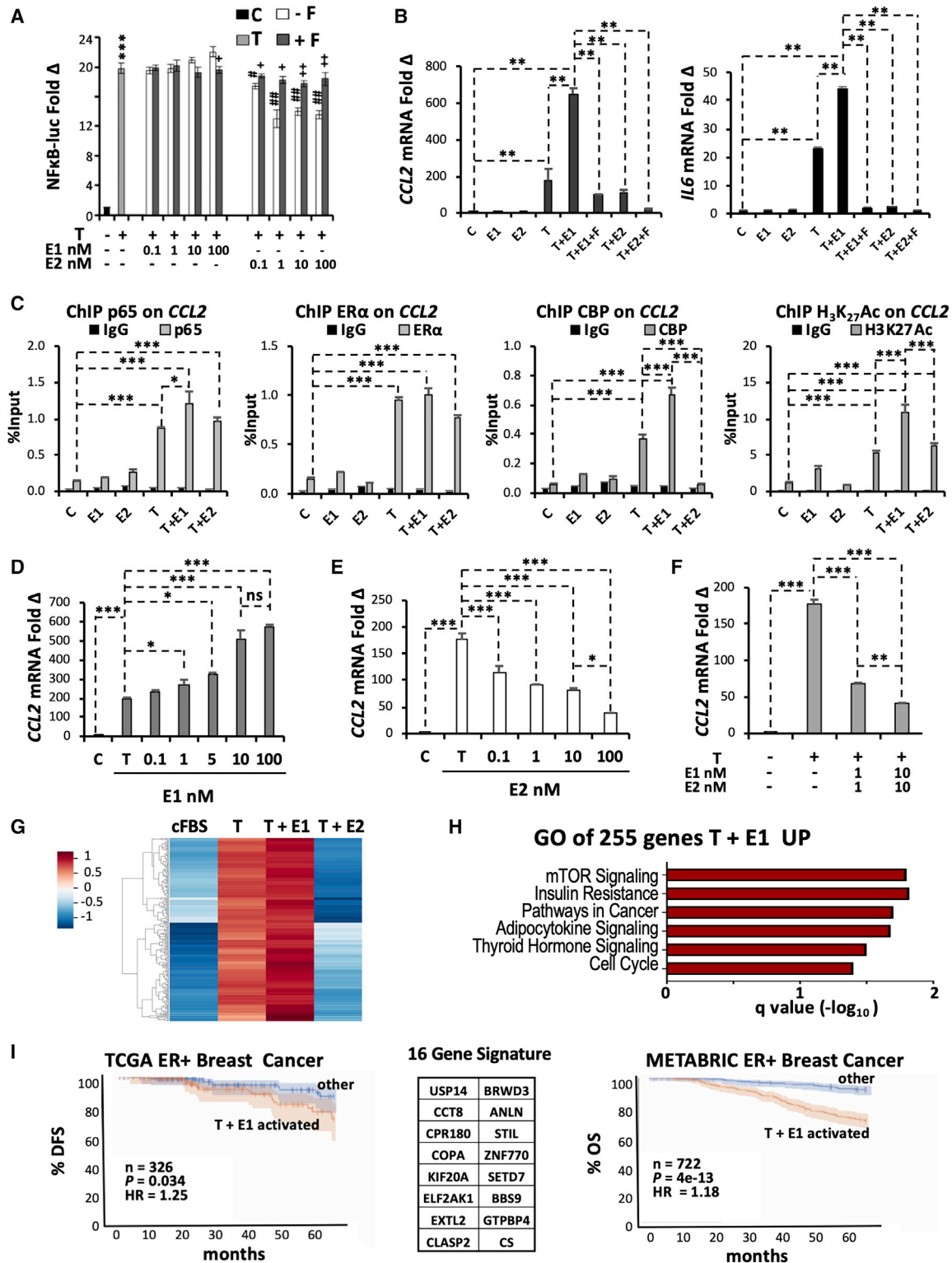


Figure 3. Estrone Cooperates with NFκB to Induce Cytokine Genes in ER+ Breast Cancer Cells

(A) NFκB luciferase activity relative to pRL in estrogen-starved MCF7 treated 8 h with vehicle (C), 10 ng/mL TNFα (T) alone, or T plus the indicated concentration of E1 or E2 added with (+F) or without (–F) prior addition of 10 nM fulvestrant (F), graphed as mean ± SEM ratio of expression versus GAPDH normalized to 1 for vehicle controls (n = 3; ***p < 0.001 versus C; #p < 0.05, ##p < 0.01 versus T; +p < 0.05, 2+p < 0.01 versus –F).

(B and C) Estrogen-starved MCF7 (C) were treated with 10 ng/mL TNFα (T) alone, with either E1 or E2 alone at 10 nM or with T+E1 or T+E2, with or without fulvestrant (F, 10 nM) for 8 h, then *CCL2* (B, left) or *IL6* (B, right) expression was assayed by qPCR. ChIP-PCR assayed p65, ERα, CBP recruitment, and H3K27Ac

(legend continued on next page)

(ChIP)-PCR in MCF7. While E1 and E2 each had little effect alone, TNF α stimulated ER α and p65 binding by 3 h. Notably, recruitment of p65 and coactivator CBP and histone H3K27 acetylation were significantly greater with TNF α +E1 than TNF α alone and were decreased by TNF α +E2 (Figure 3C). Similarly, E1 stimulated TNF α -driven ER α and CBP recruitment and H3K27 acetylation at a site -600 bp of the *IL6* transcriptional start site, while E2 markedly reduced CBP recruitment (Figures S2C and S2E). Binding of p65, ER α , and CBP to non-specific control sites was not observed for either gene (Figure S2D). Thus, *CCL2* and *IL6* both appear to be regulated by a κ B/ER α complex in which E1 stimulates and E2 disrupts coactivator CBP recruitment and gene expression (see model, Figure S2F).

ER+ breast cancer cell lines are grown in receptor-saturating doses of 10 nM E2 (Engel et al., 1978; Lippman et al., 1976, 1977; Sasson and Notides, 1983; Strobl and Lippman, 1979). However, this is higher than the 1.0–1.4 nM (or 270.3–378.5 pg/mL) concentrations of E1 and E2 observed in postmenopausal breast cancer tissue (Bonney et al., 1983; Pasqualini et al., 1996). Thus, E1 and E2 effects on TNF α -stimulated *CCL2* expression were assayed over a 4 log range of concentrations above and below those observed in normal and malignant postmenopausal breast tissue (Bonney et al., 1983; Pasqualini et al., 1996). At all concentrations tested, E2 opposed and E1 stimulated TNF α -mediated induction of both *CCL2* and *IL6* genes (Figures 3D, 3E, and S2G). Thus, even at the lower concentrations observed in normal and cancerous human breast tissues, E2 appears to have a potent anti-inflammatory effect, whereas the pro-inflammatory action of E1 rises steeply at concentrations detectable in human breast cancers after menopause, particularly in obesity.

In a competition experiment, estrogen-deprived cells were stimulated with vehicle or TNF α for 30 min and then treated with both E1 and E2 together at either 1 nM (approximating cancer tissue concentrations for both) or 10 nM (receptor-saturating concentrations for both). At both 1 and 10 nM, E2 dominated, attenuating the stimulatory effect of E1 on TNF α -mediated *CCL2* induction expression (Figure 3F). Thus, the loss of ovarian E2 after menopause would remove its restraining effect on these and potentially other E1-driven pro-inflammatory genes in the breast.

Having evaluated E1 and E2 actions in the context of NF κ B activation at κ BRE sites, we next compared E1 and E2 at classical EREs without pro-inflammatory TNF α co-stimulation. Notably, titration of E1 and E2 in ERE luciferase assays across 4 logs of ligand concentration showed greater activation by E2 than E1 at lower concentrations (0.1 and 1 nM) with maximal

E2 action by 1 nM (Figure S3A). Estrogen-stimulated ER α and SRC3 binding and H3K27 acetylation were assayed by ChIP-PCR at well-characterized ERE motifs on classic ER α target genes, *PS2* and *GREB1*. At both target gene EREs there was no significant difference between 10 nM E1- or E2-stimulated ER α and SRC3 recruitment or H3K27 acetylation (Figures S3B and S3C). At this estrogen concentration, expression of both genes was also similar (Figure S3D). Titration of E1 and E2 showed both ligands activate ERE-bearing ER α targets, *PS2*, *GREB1*, and *PGR*. E2-mediated activation peaked between 0.1 and 1 nM E2 without significant increase between 1 and 100 nM for *PGR* and *GREB1* (Figure S3B). In contrast, E2-driven *PS2* expression increased progressively at concentrations between 0.1 and 100 nM. Although E1 is a weaker ER α ligand than E2 in Scatchard analysis *in vitro* (Sasson and Notides, 1983), E1 effects on *PS2* and *GREB1* were similar to those of E2 at most concentrations in cells (Figure S3D). At the supraphysiological 100 nM concentration, E1 mediated greater induction, but this is beyond E1 steroid concentrations observed in the human breast. E2 showed greater *PGR* activation at 0.1–10 nM than E1. As for E2, actions of E1 on ERE luciferase activity and ERE target gene expression were inhibited by fulvestrant and are thus ER-dependent (Figure S3E).

To further investigate how these estrogens affect gene expression in the context of inflammation, estrogen-deprived cells were stimulated with either DMSO vehicle alone or TNF α followed by DMSO, 10 nM E1, or E2 30 min later, and global gene expression was profiled by RNA-seq at 8 h. TNF α addition led to marked changes in E1- and E2-driven gene expression (Figure S3F). To test if TNF α +E1-driven genes might have oncogenic actions not shared by TNF α +E2, we carried out GO analysis of a subset of 255 genes showing significantly greater induction with TNF α +E1 than with TNF α alone that were not upregulated by TNF α +E2 (Figures 3G and 3H). These gene sets include mTOR, insulin, and adipocytokine signaling; pathways in cancer; TSH; and cell cycle (Figures 3H and S3E), supporting the notion that in the context of inflammation, E1 drives expression of pro-oncogenic genes.

The 255 TNF α -driven genes that were further upregulated by E1, but not by E2, were analyzed for prognostic importance in newly diagnosed ER+ breast cancers from the Cancer Genome Atlas (TCGA). A 16 gene signature was identified whose upregulation in ER+ breast cancers correlated with reduced disease-free survival (HR 1.25, $p < 0.034$, $n = 326$) (Figure 3I, left). This E1+ TNF α activated gene set was validated in a larger, independent ER+ breast cancer patient cohort ($n = 722$) from the METABRIC database, with HR 1.2 and $p = 4E-13$ for decreased

at a site $-2,600$ bp of the *CCL2* transcription start site in estrogen-starved MCF7 (controls, C) treated with 10 ng/mL TNF α (T), with either 10 nM E1 or E2 alone for 3 h or with T \times 30 min followed by estrogens (T+E1 or T+E2) and recovered at 3 h (C).

(D and E) Estrogen-starved MCF7 (C) were treated with T alone, or with increasing estrogen concentrations (E1 in D; E2 in E) for 8 h followed by qPCR for *CCL2*. (F) Estrogen-starved MCF7 controls were treated with 10 ng/mL T alone or with T plus both E1 and E2 together at either 1 or 10 nM for 8 h, followed by qPCR for *CCL2*.

(B–F) Graphed as mean \pm SD for at least 3 repeat biologic experiments, each with technical triplicates, * $p < 0.05$, ** $p < 0.01$, *** $p < 0.001$.

(G and H) RNA-seq of estrogen-starved MCF7 (cFBS) treated with either DMSO vehicle alone or with T 10 ng/mL alone + DMSO, or T + 10 nM E1 (T+E1) or T + 10 nM E2 (T+E2) for 8 h. Heatmap of differentially expressed genes ($q < 0.05$) (G), and GO analysis of genes induced more with E1+T versus T and not upregulated by T+E2 (H).

(I) Kaplan Meyer plots of 16 gene signature derived from (H) versus outcome for ER+ breast cancers from TCGA (left) and METABRIC (right).

See also Figures S2 and S3.

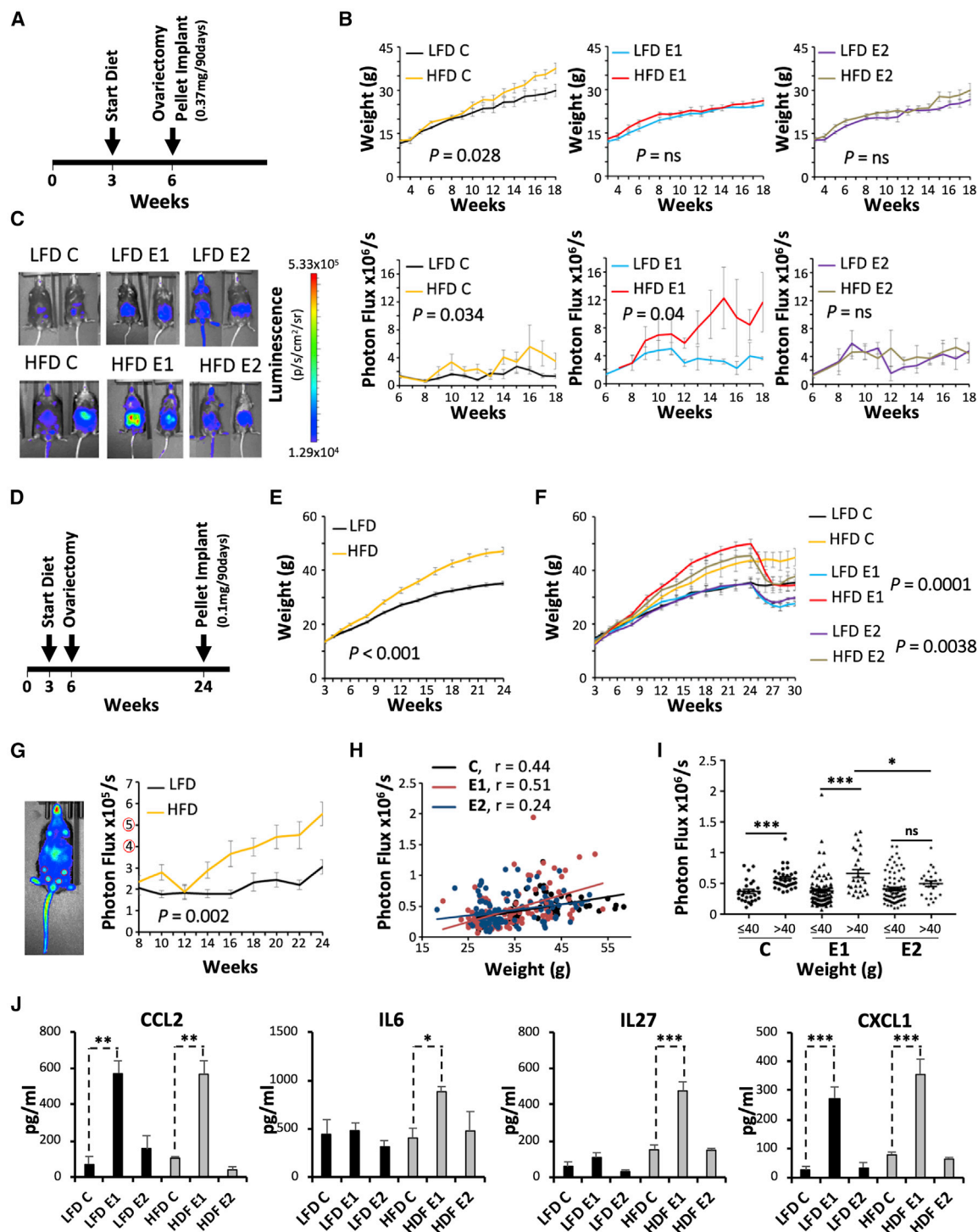


Figure 4. Estrone, but Not Estradiol, Promotes Obesity-Mediated NFκB Activation In Vivo

(A) Protocol followed in (B) and (C).

(B) Mean weights (top) and mean total photon flux/mouse by IVIS (bottom) for mice fed LFD or HFD and implanted with placebo (control, left), E1 (middle), or E2 (right) pellets are graphed as mean ± SEM (n = 10 mice/group).

(C) Representative IVIS image at week 18.

(D) Protocol followed for (E)–(J).

(E) Mean weights of LFD- and HFD-fed mice before pellet implant are graphed as mean ± SEM (n ≥ 25/group).

(F) Mean weights of LFD- or HFD-fed mice implanted with placebo (control, C), E1, or E2 pellets are graphed as mean ± SEM (n = 10).

(legend continued on next page)

overall survival (Figure 3I, right). Thus, genes activated by E1 in the presence of inflammation correlate with poor patient outcome, supporting the relevance of these pathways to ER+ breast cancer biology.

Estrone, but Not Estradiol, Cooperates with Obesity to Activate the NF κ B Pathway *In Vivo*

To investigate pro-inflammatory effects of E1 relevant to postmenopausal obese women, effects of E1 and E2 on obesity-associated inflammation were modeled *in vivo* in female B10 Cg-H2k Tg(NF κ B /Fos-luc)26Rinc/J mice that express transgenic luciferase driven by two κ BREs. Three-week-old mice were allocated to either LFD or HFD. Mice were ovariectomized at week 6 and implanted with E1 or E2 pellets or no estrogen-control pellets (Figure 4A). Notably, both E1 and E2 protected against HFD-induced weight gain, providing a biomarker of *in vivo* activity (Figure 4B). NF κ B luciferase activity was measured by *in vitro* imaging system (IVIS). HFD-induced obesity alone activated NF κ B (luciferase activity photon flux; Figures 4B, bottom left panel, and 4C). Interestingly, E2 inhibited NF κ B activation by obesity, whereas the dominant postmenopausal estrogen, E1, significantly increased obesity-mediated inflammation (Figures 4B and 4C).

Since HFD-induced weight gain was impeded by estrogen supplementation, a second experiment randomized mice to LFD or HFD for 24 weeks to permit weight gain before estrogen pellet implantation (Figures 4D and 4E). E1 and E2 supplementation at week 24 led to weight loss in both groups (Figure 4F). To specifically evaluate mammary tissue NF κ B activity, inguinal mammary gland luminescence was quantitated. HFD increased mammary gland NF κ B activity even without estrogen supplementation (Figures 4G and S4A–S4C). Mammary NF κ B activity was highest in E1-treated mice and was decreased by E2 supplementation compared to no estrogen controls (Figure S4A). Mammary-specific bioluminescence showed linear relationship between weight gain and NF κ B activity, with an increased slope and correlation coefficient for E1 ($r = 0.51$) versus control ($r = 0.44$) and a diminished slope for E2 ($R = 0.24$) (Figures 4H and S4C). All HFD mice were obese by 24 weeks. Obese mice (>40 g) in both HFD control and HFD + E1 groups showed higher NF κ B activity. E2 was protective, with significantly lower inflammation (photon flux) in mammary glands of HFD + E2-supplemented obese mice than with HFD + E1 (Figure 4I).

HFD also induced NF κ B activation in abdominal fat. As for mammary tissue, E2-supplemented mice had significantly lower abdominal luminescence than HFD-induced obese control and obese E1 mice (Figures S4D–S4G). Here also, there was a linear relationship between inflammation (total photon flux) and weight increase, with the highest correlation in E1-

supplemented mice, followed by no-estrogen controls, then E2 implanted mice (Pearson coefficient; Figures S4F and S4H). When mice were dichotomized by weight above or below 40 g, obesity increased abdominal inflammation in all groups (control, E1, and E2), with E2 supplements decreasing inflammation in obese abdomens compared to no estrogen controls and obese E1-treated (Figure S4I).

Serum levels of several pro-inflammatory cytokines, assayed at the end of this experiment, were increased in HFD + E1 mice compared to HFD + E2 and LFD groups. Notably, circulating CCL2 and CXCL1 increased with E1 in both LFD and HFD groups (Figure 4J). These data strongly support a pro-inflammatory role for E1 in obesity-mediated NF κ B activation and indicate a protective effect of E2.

HSD17B14 Overexpression Increases Intracellular Estrone, Inflammation, and CSC Properties in ER+ Breast Cancer Cells

Several 17 β -hydroxysteroid dehydrogenase (HSD17B) family enzymes convert intracellular E1 to E2 and vice versa in human tissues including mammary fat (Hilborn et al., 2017). We reasoned that since E1 stimulates pro-inflammatory, pro-oncogenic genes not activated by E2, enzymes converting E2 to E1 might be overexpressed in aggressive ER+ breast cancers. The prognostic import of HSD17B family members was evaluated in the KM Plotter primary human breast cancer database. Of these, high expression of *HSD17B14*, which converts E2 to E1, was prognostic of poor survival in women with ER+ breast cancer (HR 1.59, $p = 0.0058$; Figure 5A). Analysis of TCGA data shows *HSD17B14* levels are higher in breast cancers (all subtypes, $n = 1,097$, $p = 1.44329E-15$) and even more so in ER+ luminal cancers ($n = 566$, $p = 9.312218E-12$) than in normal mammary tissues ($n = 114$) (Figure S5A). Notably, *HSD17B14* expression was also higher in ER+ breast cancer lines than in the immortal, non-tumorigenic ER+ mammary epithelial MCF12A line (Figure S5B). Finally, *HSD17B14* expression was also greater in cancer-associated mammary adipocytes (Ca) than contralateral unaffected tissue (N) in women undergoing bilateral mastectomy for unilateral breast cancer (Figure 5B). These observations in clinical patient tissues led us to test the effects of HSD17B14 upregulation in ER+ breast cancer models.

HSD17B14 overexpression was assayed in three ER+ lines (MCF7, T47D, and MDA-MB-361). *HSD17B14* overexpression (shown in Figure S5C) decreased intracellular E2, increased intracellular E1, and increased expression and secretion of pro-inflammatory cytokines in all three *HSD17B14*-transduced lines (Figures 5C–5E, S5D, and S5E; fold changes in cytokine shown in Table S3). The upregulation of *CCL2*, *IL6*, and *IL8* expression in MCF7-HSD17B14 (MCF7HSD) compared to vector controls was inhibited by 10 nM fulvestrant treatment for 48 h (Figure 5D). Global expression profiling of MCF7HSD versus

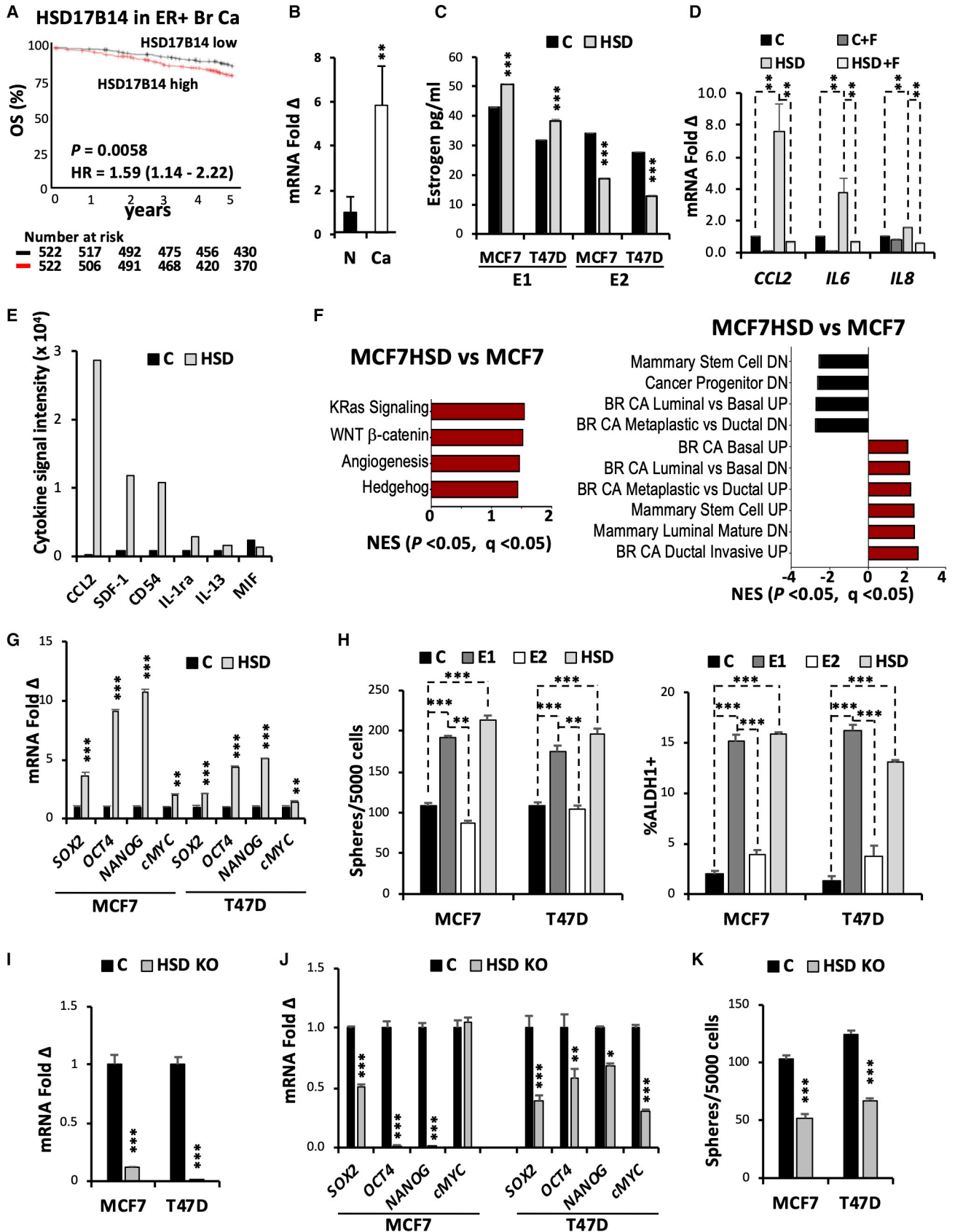
(G) Representative IVIS image shows mammary glands 4 and 5 selected for analysis (left). Mean total photon flux/mouse by IVIS (right) for LFD- and HFD-fed mice before pellet implant is graphed \pm SEM ($n \geq 25$, pooled data from LFD and HFD).

(H) Correlation between individual mouse weights and photon flux by IVIS after pellet implant.

(I) Total photon flux/mouse from mammary glands 4 and 5 graphed for non-obese (≤ 40 g) and obese (>40 g) mice in placebo (control, C), E1-treated, or E2-treated mice, graphed as mean \pm SEM ($n \geq 10$; * $p < 0.05$, *** $p < 0.001$).

(J) Serum cytokine concentrations assayed by Luminex Bio-Plex 200 are graphed as mean \pm SEM ($n \geq 3$; * $p < 0.05$, *** $p < 0.001$).

See also Figure S4.



(legend on next page)

MCF7 controls showed activation of oncogenic signaling, a shift from luminal to basal gene expression, and upregulation of mammary stem cell profiles (Figures 5F and S5F; Table S4). In all three cancer lines, HSD17B14-driven cytokine upregulation led to increased expression of ESC-TFs *SOX2*, *OCT4*, *NANOG*, and *MYC* (Figures 5G, S5G, and S5H). Notably, E1 treatment and HSD17B14 overexpression increased both sphere-forming and ALDH1+ cells, and E2 decreased both in MCF7 and T47D (Figures 5H and S5I). CRISPR knockdown of HSD17B14 (Figures 5I and S5J) decreased cytokine and stem cell factor expression and sphere formation compared to vector controls, consistent with a reduced stem cell-like population (Figures 5J, 5K, and S5K). Thus, both E1 exposure and HSD17B14, which converts intracellular E2 to E1, upregulate inflammatory cytokines and CSC-like properties *in vitro*.

High Intratumor E1:E2 Increases Tumor-Initiating Stem Cells and Tumor Growth *In Vivo*

To date, E2 supplements have been used to support human ER+ breast cancer culture and xenograft growth. Here we compared effects of E1, E2, and constitutive intra-tumor E2 conversion to E1 by HSD17B14 on tumor-initiating stem cells (T-ISCs) and tumor growth in vector control MCF7 and MCF7HSD orthotopic xenografts in NODSCID mice (n = 8/group). MCF7 xenografts had longer latency and grew more slowly with E2 than with E1 pellets. MCF7HSD emerged most rapidly and grew faster with either E1 or E2 pellets (Figures 6A and S6A). E2-supplemented MCF7 had the highest intra-tumor E2 and lowest E1 concentrations (Figure 6B). E1 was high in E1-supplemented MCF7 tumors and, as predicted, in MCF7HSD xenografts supplemented with either E1 or E2 (Figure 6B). All three E1-driven tumor groups showed reduced intratumor E2 concentrations, with the lowest E2 in MCF7HSD tumors (Figure 6B). Thus, the most rapidly growing tumors had the highest E1:E2 ratio. All tumor groups had similar cell proliferation as indicated by %Ki67 staining (Figure S6B). Notably, both MCF7 and MCF7HSD were estrogen dependent since mice injected with no-estrogen control pellets failed to generate tumors by 12 weeks (Figure 6A). Furthermore, both E1- and E2-stimulated tumor growth is ER dependent since it was inhibited by fulvestrant administration in all groups (Figures S6C and S6D).

Circulating cytokine levels were higher in mice bearing E1-stimulated or HSD transduced MCF7 tumors than with

E2-supplemented tumors (representative data; Figure 6C). Three tumors from each experimental group in Figure 6A were dissociated, and single-cell suspensions were pooled and assayed for ALDH1 activity or implanted in secondary hosts in limiting dilutions (n = 8/group) to quantitate T-ISCs. ALDH1+ cells and T-ISCs were least abundant in E2-supplemented tumors, and significantly increased in E1-supplemented tumors (Figure 6D). MCF7HSD tumors supplemented with either estrogen had the highest ALDH1+ cell and T-ISC abundance, generating more tumors with shorter latency in secondary hosts (Figures 6D–6F). RNA-seq of xenograft tumors showed marked differences in gene expression between E2-supplemented and E1-driven tumors (Figure S6E). Gene set enrichment analysis (GSEA) showed that all three tumor groups with high E1 and relatively low E2 showed a shift from luminal to basal profiles, activation of mammary stem cell programs, and poor prognosis metaplastic and invasive cancer signatures compared to E2-supplemented cancers (Figures 6G–6I and S6F).

To further validate the unprecedented finding that the dominant postmenopausal estrogen, E1, is more tumorigenic than E2, effects of these hormones were tested on a second, independent estrogen-sensitive mammary tumor model, E0771. This syngeneic ER+ mammary tumor model also showed faster growth with E1 supplementation than E2 *in vivo*. Moreover, fulvestrant opposed both E1- and E2-mediated E0771 tumor growth in this second, somewhat more resistant model system (Figures 7A and 7B). Serum cytokine assays from E0771 tumor-bearing mice confirm that E1-driven tumors cause greater systemic cytokine upregulation than observed with E2. The tumor-driven increase in circulating cytokines was ER dependent since it was opposed by fulvestrant (Figure 7C). Uterine wet weights were evaluated. Both E1- and E2-treated mice showed a significant increase in uterine weight, providing a biomarker of steroid exposure in estrogen-treated groups versus sham pellet controls (Figure 7D).

DISCUSSION

While estrogens promote ER+ breast cancer growth (Engel et al., 1978; Knazek et al., 1977; Lippman and Allegra, 1978) and anti-estrogen therapies are a mainstay of patient care (Ma et al., 2015), paradoxically, breast cancer risk increases after menopause when estrogen levels decline. ER+ breast cancer risk increases with obesity after menopause but is decreased in obese

Figure 5. HSD17B14 Overexpression Increases Intracellular Estrone, Inflammation, and Stem Cell-like Properties in ER+ Breast Cancer Cells

- (A) KM plotter analysis of *HSD17B14* expression versus ER+ breast cancer survival.
 (B) *HSD17B14* expression in peritumoral (Ca) or contralateral unaffected “normal” (N) breast fat from bilateral mastectomy patients, graphed as mean ± SEM ratio of expression versus GAPDH normalized to 1 for vehicle controls.
 (C) E1 and E2 concentrations (pg/mL) in MCF7 and T47D control (C) or *HSD17B14* overexpressing lines (HSD).
 (D) Cytokine expression assayed by qPCR in MCF7 control (C) or MCF7HSD (HSD) with or without addition of 10 nM fulvestrant (+F) for 48 h.
 (E) Conditioned media from triplicate MCF7 versus MCF7HSD collected after 5 days were pooled and evaluated on a single Human Cytokine Array (R&D Systems). Secreted cytokine levels are expressed as arbitrary intensity units versus 1 for controls.
 (F) GO analysis of differentially expressed genes in MCF7HSD versus MCF7 vector controls.
 (G and H) ESC-TF levels (G), spheres (H, left), and %ALDH1+ cells (H, right) in MCF7 and T47D controls (C) treated with either E1 or E2 and in *HSD17B14* overexpressing lines (HSD).
 (I–K) MCF7 and T47D vector control lines were compared to *HSD17B14* CRISPR knockout (HSD KO) for expression of *HSD17B14* (I), for ESC-TF (J) graphed as mean ± SEM ratio of expression versus GAPDH normalized to 1 for vehicle controls (C), and for sphere formation (K).
 All graphed data except for (E) show mean for at least 3 repeat biologic experiments (each with technical triplicates for qPCR, mean ± SEM, *p < 0.05, **p < 0.01, ***p < 0.001). See also Figure S5 and Tables S3 and S4.

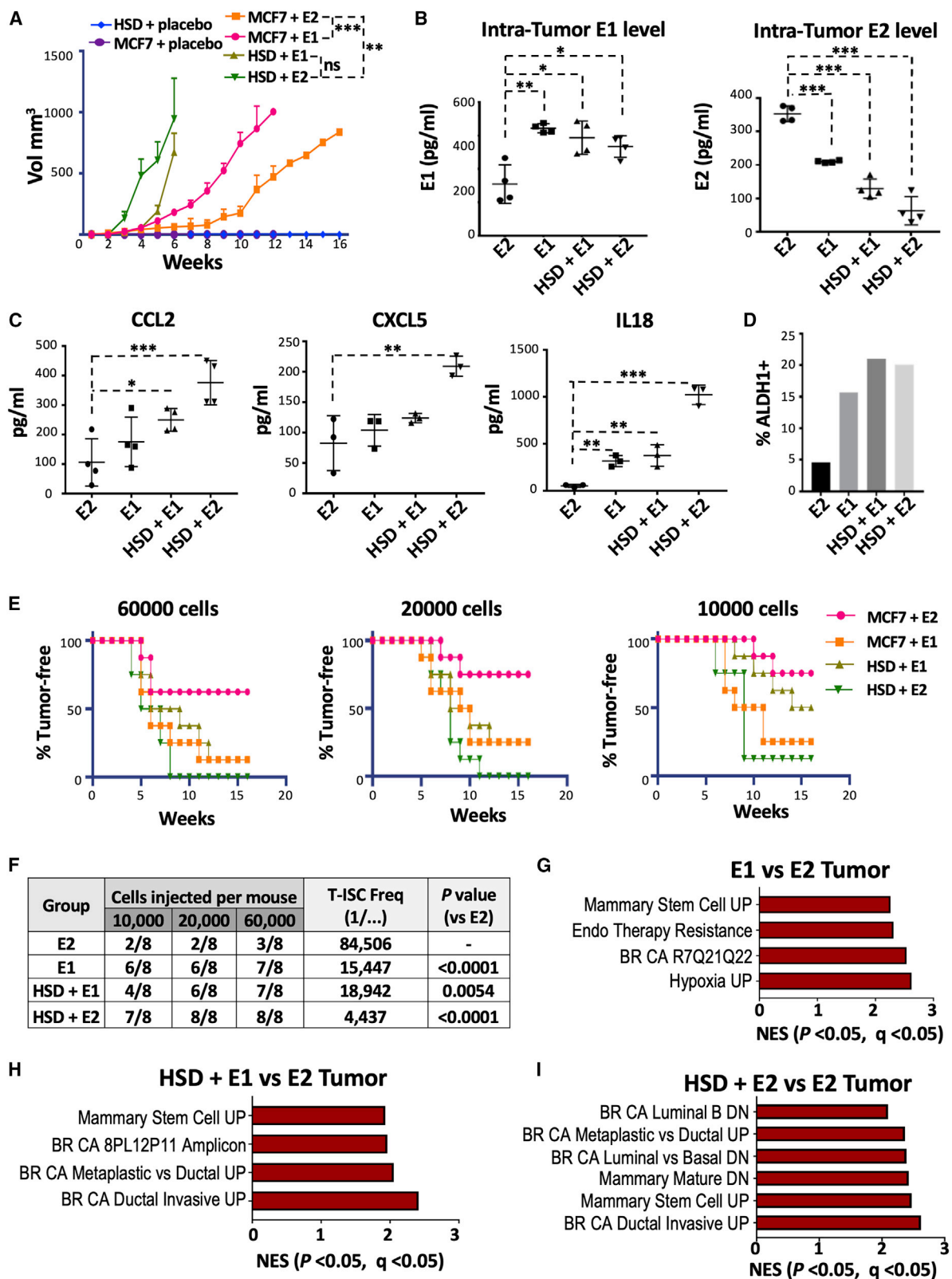


Figure 6. High Intratumor E1:E2 Increases Tumor Growth and Tumor-Initiating Stem Cells *In Vivo*

(A) Mean tumor volume/time is graphed for MCF7 vector controls (C) or MCF7HSD in NOD-SCID mice supplemented with E1, E2, or placebo control pellets (n = 8/group, *p < 0.05, **p < 0.01, ***p < 0.001). See also Figures S6A–S6D.

(legend continued on next page)

premenopausal women, suggesting an important interplay between estrogens and obesity. In contrast to the anti-inflammatory action of ovarian E2 (Kalaitzidis and Gilmore, 2005), here, we show that the dominant postmenopausal estrogen, E1, is proinflammatory and that increased E1 levels in breast and adipose tissue after menopause might contribute to the excess development and adverse outcome of ER+ breast cancer in obesity.

Circulating inflammatory cytokines increase with age (Bruunsgaard et al., 2001) and rise after menopause (Pfeilschifter et al., 2002) and with obesity (Picon-Ruiz et al., 2017), and their expression in breast cancer tissue correlates with poor outcome (Nicolini et al., 2006; Soria and Ben-Baruch, 2008; Waugh and Wilson, 2008). In obese adipose tissue, abundant pre-adipocytes secrete cytokines that activate NFκB and recruit additional inflammatory mediators (Picon-Ruiz et al., 2017). In obese fat, inflammation is manifest by crown-like structures (CLSs) of macrophages surrounding dying adipocytes (Quail and Dannenberg, 2019). CLS prevalence in mammary tissue increases after menopause (Iyengar et al., 2015) and with obesity (Morris et al., 2011). CCL2, IL6, and IL8 exposures all increase breast CSC-like cells (Ginestier et al., 2010; Picon-Ruiz et al., 2016; Sansone et al., 2007; Tsuyada et al., 2012). Here, we show that inflammatory cytokine production in human mammary adipocytes increases with obesity, after menopause, and in proximity to cancers. Interaction of these more inflammatory adipocytes with cancer cells stimulates E1- and NFκB-dependent cytokine induction and expansion of stem-like cancer cells.

We make the unprecedented observation that the dominant pre- and postmenopausal estrogens, E2 and E1, respectively, appear to have different effects on NFκB-driven inflammation. Here, we report that NFκB-mediated inflammation accompanying chronic hypercaloric stress in mice is relieved by E2, but not by E1. The effects of E1 on gene expression have not been extensively assayed. In primary human adipocytes and in three ER+ breast cancer models, we show that gene expression programs activated by E1 and E2 are not identical. While they activate many common pathways, genomic profiling shows for the first time that E1 on its own promotes NFκB activation. Ovarian E2 opposes NFκB activation (reviewed in Kalaitzidis and Gilmore, 2005), and this is thought to underlie the neuro- and cardio-protective effects of ovarian estrogens in younger women. E2 opposes NFκB activation by multiple cell-type-dependent mechanisms, including *IκB* induction and activation, *IKK* repression, and decreased nuclear p65 translocation (see Baumgarten and Frasor, 2012; Kalaitzidis and Gilmore, 2005 for reviews). E2-liganded ERα disrupts κBRE-bound p65 at *IL6*, *CCL2*, and/or *TNFα* promoters (Giraud et al., 2010; Nettles et al., 2008; Stein and Yang, 1995) and can increase corepressor (Cvoro et al.,

2006; Nwachukwu et al., 2014) or decrease coactivator recruitment (Nettles et al., 2008; Nwachukwu et al., 2014). These effects involve ERα since they are mediated by ERα-specific, but not ERβ-specific, ligands and abrogated by *ESR1* knockdown (Giraud et al., 2010; Stender et al., 2017). Upon treatment with TNFα and E2, p65 acts as a pioneer factor, shifting ERα from largely ERE sites in the presence of E2 alone to κBRE sites (Pradhan et al., 2010) to remodel FoxA1-dependent ERα recruitment to chromatin (Franco et al., 2015). Not only does E2-bound ERα oppose NFκB action, but NFκB also modulates ERα action in part by changing the ERα-regulated transcriptome (Frasor et al., 2009, 2015; Stender et al., 2017).

In the presence of TNFα, the transcriptomes activated by E1 and E2 differ. E1-bound ERα stimulates recruitment of coactivator, CBP, and H3K27 acetylation to increase TNFα-driven κB induction of *IL6* and *CCL2*, while E2 opposes it. Indeed, a subset of TNFα-activated genes that are further induced by E1, but not by E2, drive gene expression profiles of poor prognostic import in two independent ER+ breast cancers cohorts, providing evidence that E1-activated proinflammatory genes are germane to the human disease under study. NFκB is oncogenic in the breast. Aberrant activation of NFκB in murine mammary epithelium leads to spontaneous mammary tumor development (Barham et al., 2015; Romieu-Mourez et al., 2003). NFκB activation in ER+ cancers is prognostic of poor outcome and drives endocrine therapy resistance (Sas et al., 2012), in part through TNFα-stimulated IKKβ phosphorylation of ERα at S305 leading to ligand-independent ERα activation (Stender et al., 2017). While most NFκB-activated genes are downregulated by E2, Frasor et al. identified a subset of E2 + TNFα-upregulated genes that are overexpressed in aggressive ER+ breast cancers and that correlate with poor outcome (Frasor et al., 2009). Present work further illuminates pro-tumorigenic NFκB actions. In the context of obesity and high E1, a novel program of pro-oncogenic TNFα-activated genes is further upregulated.

Although E1 is a relatively weak estrogenic ligand, with nearly a log fold lower binding affinity for ERα *in vitro* than E2 (Sasson and Notides, 1983), its *in vivo* actions might be more consequential than predicted by its weak receptor binding. While E1 differs from E2 in its interaction with ERα at κBRE sites, many genes are altered by both ligands and E1 and E2 actions appear remarkably similar at the classic ERE-driven genes evaluated herein. A similar magnitude of E1 and E2 action on *PGR* expression was reported in ovarian cancer cells (Mukherjee et al., 2005). The greater than expected potency of E1 *in vivo* might result from its ready conversion to E1 sulfate, whose metabolic clearance from serum (and hence tissues) is lower than that of E1 (Siteri and MacDonald, 1973). Furthermore, whereas E2 binding activates receptor proteolysis, thereby curtailing ERα

(B) Mean ± SEM intratumoral E1 and E2 levels (pg/mL) in indicated xenograft tumors (n ≥ 3, *p < 0.05, **p < 0.01, ***p < 0.001).

(C) Proinflammatory cytokine proteins were assayed using Luminex Bio-Plex 200 (as described in STAR Methods) in serum from at least 3 tumor bearing mice/group and graphed as mean ± SEM (*p < 0.05, **p < 0.01, ***p < 0.001).

(D–F) Xenograft tumors were removed when they reached 1 cm, and dissociated tumor cells from at least 3 mice were pooled and assayed for ALDH1 activity (% ALDH1+) (D) or implanted in limiting dilutions into recipient NSG mice (n = 8/group) and tumor emergence over time/implantation group (E) and T-ISC quantitation (F) are shown.

(G–I) RNA-seq was carried out on ≥ 3 tumors/group from the experiment in (A) above. GO analysis shows enrichment of mammary stem cell gene profiles and a shift from luminal to basal gene expression in tumors driven by high E1 and low E2 compared to high E2 and low E1.

See also Figure S6.

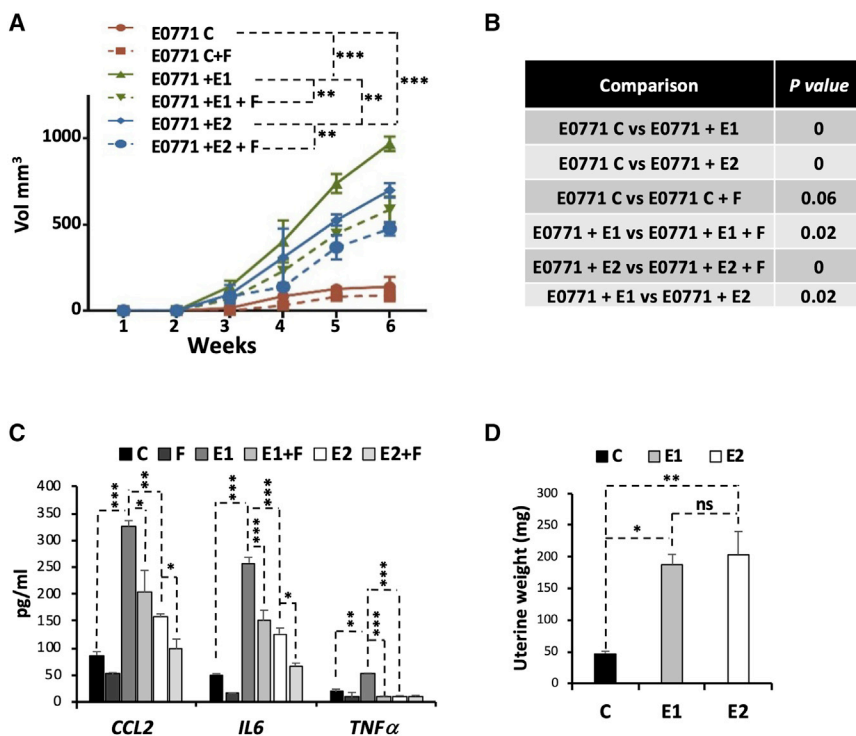


Figure 7. E1 Induced Greater Tumor Growth Than E2 in E0771 and Both Estrogens Were Inhibited by Fulvestrant

(A) Mean tumor volume/time is graphed for E0771 implanted into C57BL/6 mice supplemented with E1, E2, or placebo control (C) pellets as described in STAR Methods (n = 5/group; **p < 0.01, ***p < 0.001). Mice were treated with fulvestrant (F) as described.

(B) Statistical data from the comparison of growth curves shown in (A).

(C) Pro-inflammatory cytokine proteins were assayed using Luminex Bio-Plex 200 (as described in STAR Methods) in serum from at least 3 tumor-bearing mice/group and graphed as mean ± SEM (*p < 0.05, **p < 0.01, ***p < 0.001).

(D) Uterine weights in C57BL/6 mice supplemented with E1, E2, or placebo control pellets. (*p < 0.05, **p < 0.01, ***p < 0.001).

transcriptional activity, this might not be the case with E1. Limited preliminary data suggest E1 does not mediate receptor degradation, which would lead to a more sustained E1:ER α transcriptional activity. Oncogenic pathways that reduce E1 conversion to E2 could also raise local E1 concentrations in the breast. Interestingly, the most abundant HSD isoform in the normal breast is HSD17B1, which converts E1 to E2 (Hilborn et al., 2017). Our review of publicly available TCGA data from primary human breast cancers showed that *HSD17B1* expression is significantly lower in ER+ breast cancers than in normal breast tissue (data not shown). Local E1 levels in premalignant or cancerous breast tissue could also be increased by the oncogenic induction or overactivation of HSDs converting E2 to E1.

The balance of E1 and E2 appears to critically modulate breast cancer growth *in vivo*. HSD17B14, which converts E2 to E1 (Hilborn et al., 2017), is more highly expressed in ER+ breast cancers than in normal breast tissue, associates with poor ER+ breast cancer outcome, and is oncogenic in ER+ breast cancer lines. For nearly a half century, since estrogens were identified as essential ER+ breast cancer mitogens (Engel et al., 1978; Knazek et al., 1977; Lippman et al., 1976; Lippman and Allegra, 1978), E2 has been used in experimental research. To our knowledge, we present herein the first comparison of E1 and E2 actions on tumor growth. *HSD17B14* overexpression increased intracellular E1 and decreased E2. Both E1 treatment and *HSD17B14* overexpression increased ALDH1 activity and tumorspheres, while E2 and *HSD17B14* knockdown did the inverse. E1 supported faster tumor emergence and growth *in vivo* than E2 in two independent models and acts via the ER since fulvestrant opposed tumor growth. MCF7HSD tumors had high E1 and low E2 levels, reflecting avid E2 conversion to E1, and their growth, while estrogen dependent, was more rapid with either

the doubling of circulating E1 levels in obesity (which reflects up to 6-fold higher E1 levels within the breast tissue) correlates with an over 2-fold increase in risk of ER+ breast cancer in both Caucasian (Kaaks et al., 2005; Key et al., 2015) and Asian (Miyoshi et al., 2003; Yu et al., 2003) postmenopausal women. Thus, E1 appears to drive ER+ CSC expansion and tumor growth *in vivo*, and we cautiously suggest that the balance of these estrogens, with a high E1:E2 ratio, might be critical for tumorigenesis.

While adrenal androstenedione production does not differ between obese and normal weight women, peripheral conversion of adrenal androstendione to E1 is doubled in obese women, due largely to the increase in aromatase-rich adipose tissue (Sii-teri and MacDonald, 1973). The inflammatory milieu of obesity further drives E1 synthesis via IL6- and TNF α -mediated induction of aromatase expression (Purohit et al., 2002; Purohit and Reed, 2002). After menopause, weight gain is frequent, due in part to loss of E2-mediated adiponectin gene induction and leptin gene repression (Picon-Ruiz et al., 2017). Weight gain after menopause is associated with increased ER+ breast cancer risk and mortality (Demark-Wahnefried et al., 2012; Nichols et al., 2009; Vance et al., 2011). Notably, over 79% of breast cancer patients are overweight or obese at diagnosis (Ligibel et al., 2014) and further weight gain during therapy is nearly invariable (Demark-Wahnefried et al., 2012; Nichols et al., 2009; Vance et al., 2011). Since obesity increases E1 synthesis (MacDonald et al., 1978), the excess weight gain after menopause and in postmenopausal ER+ breast cancer patients after diagnosis is not an innocuous norm, but would have deleterious consequences. E1- and NF κ B-dependent cytokine induction provides a mechanism whereby weight gain would increase ER+ breast cancer risk and worsen its outcome.

Our data provide insight into why ER⁺ breast cancer risk is increased with obesity after menopause, but not before. While high ovarian E2 would oppose the mammary inflammation of obesity before menopause, after menopause the inductive effects of E1 on inflammatory ER α / κ B targets are unopposed by E2. The opposing effects of E1 and E2 on inflammation and CSCs might also underlie the increased ER⁺ breast cancer incidence after menopause. The declining E2:E1 ratio, and the increased inflammatory cytokine milieu after menopause, particularly in overweight and obesity, would drive ER α / κ B target activation in breast epithelia and adipocytes. Upon invasion into peritumoral fat, interaction between invading breast cancer cells with E1-rich adipocytes would further activate NF κ B and inflammatory cytokines to promote CSC expansion, invasion, and metastasis (Picon-Ruiz et al., 2016).

The rise in obesity (Finkelstein et al., 2012; Ward et al., 2019) is associated with an increase in inflammation-associated diseases, including cancer (Kanneganti and Dixit, 2012; Quail and Dannenberg, 2019). Present findings provide a strong molecular rationale for lifestyle interventions in overweight breast cancer patients. They may also prove relevant to other obesity-associated diseases including diabetes, and cardiovascular and neurodegenerative diseases such as Parkinson's and Alzheimer's diseases, that increase after menopause. Finally, postmenopausal endocrine replacement therapies may warrant re-thinking, with attention to resulting levels of both E1 and E2. Our data support further research to generate safe and effective endocrine replacement modalities, and to target HSD17B enzymes to decrease E1 (Poirier, 2015), decrease breast cancer risk, and improve neurocognitive and cardiovascular health.

Limitations of Study

Present work did not include analysis of E1 and E2 pharmacokinetics, effects on tumor metastasis, or how E1 and E2 influence the tumor-promoting effects of obesity *in vivo*. Furthermore, while E1-induced cytokines increased CSC *in vitro* and *in vivo*, whether cytokine blockade abrogates E1-driven tumor formation has yet to be determined. E1 is a major driver of obesity-related inflammation, but clearly not the only mediator. While we tested how estrogen concentrations affect ER binding to and activation of a limited number of ER α / κ B and ERE-bearing target genes, how different E1/E2 ratios affect gene expression and tumor growth warrants evaluation. Further assays are needed to test how the different E1 concentrations and E1/E2 ratios observed in the human breast with and without obesity affect models of ER⁺ breast tumorigenesis *in vivo*. Finally, although we show E1- and E2-driven gene expression profiles differ and are altered by inflammation (addition of TNF α), it will be critical to understand how different ligand concentrations and E1/E2 ratios affect the extent and timing of global ER α recruitment to ERE, κ B, and other chromatin motifs and predicate differences in gene expression. Further evaluation of E1 and E2 action will undoubtedly illuminate estrogen:ER biology and its application to human disease.

STAR★METHODS

Detailed methods are provided in the online version of this paper and include the following:

- KEY RESOURCES TABLE
- RESOURCE AVAILABILITY
 - Lead Contact
 - Materials Availability
 - Data and Code Availability
- EXPERIMENTAL MODEL AND SUBJECT DETAILS
 - Human Subjects
 - Mouse Models
 - Adipocyte, SVF and hASC Isolation from Fat Tissue
 - Cell Culture
- METHOD DETAILS
 - Cytokine Assays
 - Quantitative RT-PCR (qPCR)
 - Aldehyde Dehydrogenase Activity by ALDEFLUOR Assay
 - Mammosphere-formation Assay
 - Western-Blotting
 - *In vitro* Dual Luciferase Assays
 - Estrogen Concentration Assays
 - Chromatin Immunoprecipitation Assay
 - Estrogen Regulation of Obesity-Mediated NF- κ B Activity *In Vivo*
 - Lentivirus Production and Establishment of HSD17B14 Expressing Cells
 - CRISPR Mediated HSD-17B14 Knockout Lines
 - RNA Sequencing (RNA-seq)
 - Orthotopic Tumor Formation Assays
 - Assays with Dissociated Xenograft Tumor Cells
 - Immunohistochemistry
 - RNA-seq Bioinformatic Analysis
 - Analysis of TNF α and Estrogen Regulated Genes in Primary ER⁺ Human Breast Cancers
- QUANTIFICATION AND STATISTICAL ANALYSIS

SUPPLEMENTAL INFORMATION

Supplemental Information can be found online at <https://doi.org/10.1016/j.cmet.2020.05.008>.

ACKNOWLEDGMENTS

This work was supported by grants from the Florida Breast Cancer Foundation (J.M.S.), the Breast Cancer Research Foundation (J.M.S.), the NIH (1R01CA210440-01A1; J.M.S.), the Susan G. Komen Foundation (PDF16380958; M.P.-R. and J.M.S.), and the European Commission (MSCA-IF-2018 845104; M.P.-R.). I.A.-R. and M.d.M.V. were supported by MINECO for the Severo Ochoa Excellence Accreditation (SEV-2016-0644). We thank Luis Morey for helpful discussions in the course of this work. We acknowledge assistance from the Oncogenomics, Biostatistics/Bioinformatics, and Biospecimen Shared Resources of Sylvester Comprehensive Cancer Center. Dr. Reuben Shaw is acknowledged for providing the pRL vector.

AUTHOR CONTRIBUTIONS

Conceptualization, J.M.S., M.E.L., R.Q., and M.P.-R.; Methodology, J.M.S., M.P.-R., and R.Q.; Investigation, R.Q., M.P.-R., M.D., H.Y., R.R., C.M.-T., V.N.d.P., T.I., and I.A.-R.; Validation, M.P.-R., R.Q., and J.M.S.; Formal Analysis, R.Q., M.P.-R., and J.M.S.; Writing – Original Draft, M.P.-R., J.M.S., and R.Q.; Writing – Review & Editing, J.M.S., M.P.-R., and R.Q.; Funding Acquisition and Resources, J.M.S., M.P.-R., and M.d.M.V.

DECLARATION OF INTERESTS

The authors declare no competing interests.

Received: May 31, 2019

Revised: December 26, 2019

Accepted: May 11, 2020

Published: June 2, 2020

REFERENCES

- Adly, L., Hill, D., Sherman, M.E., Sturgeon, S.R., Fears, T., Mies, C., Ziegler, R.G., Hoover, R.N., and Schairer, C. (2006). Serum concentrations of estrogens, sex hormone-binding globulin, and androgens and risk of breast cancer in postmenopausal women. *Int. J. Cancer* *119*, 2402–2407.
- Barham, W., Chen, L., Tikhomirov, O., Onishko, H., Gleaves, L., Stricker, T.P., Blackwell, T.S., and Yull, F.E. (2015). Aberrant activation of NF- κ B signaling in mammary epithelium leads to abnormal growth and ductal carcinoma in situ. *BMC Cancer* *15*, 647.
- Barton, G.M. (2008). A calculated response: control of inflammation by the innate immune system. *J. Clin. Invest.* *118*, 413–420.
- Baumgarten, S.C., and Frasor, J. (2012). Minireview: Inflammation: an instigator of more aggressive estrogen receptor (ER) positive breast cancers. *Mol. Endocrinol.* *26*, 360–371.
- Bonney, R.C., Reed, M.J., Davidson, K., Beranek, P.A., and James, V.H. (1983). The relationship between 17 beta-hydroxysteroid dehydrogenase activity and oestrogen concentrations in human breast tumours and in normal breast tissue. *Clin. Endocrinol. (Oxf.)* *19*, 727–739.
- Bruunsgaard, H., Pedersen, M., and Pedersen, B.K. (2001). Aging and proinflammatory cytokines. *Curr. Opin. Hematol.* *8*, 131–136.
- Calle, E.E., Rodriguez, C., Walker-Thurmond, K., and Thun, M.J. (2003). Overweight, obesity, and mortality from cancer in a prospectively studied cohort of U.S. adults. *N. Engl. J. Med.* *348*, 1625–1638.
- Chan, D.S., Vieira, A.R., Aune, D., Bandera, E.V., Greenwood, D.C., McTiernan, A., Navarro Rosenblatt, D., Thune, I., Vieira, R., and Norat, T. (2014). Body mass index and survival in women with breast cancer—systematic literature review and meta-analysis of 82 follow-up studies. *Ann. Oncol.* *25*, 1901–1914.
- Chen, Y., Guggisberg, N., Jorda, M., Gonzalez-Angulo, A., Hennessy, B., Mills, G.B., Tan, C.K., and Slingerland, J.M. (2009). Combined Src and aromatase inhibition impairs human breast cancer growth in vivo and bypass pathways are activated in AZD0530-resistant tumors. *Clin. Cancer Res.* *15*, 3396–3405.
- Cvoro, A., Tzagarakis-Foster, C., Tatomer, D., Paruthiyil, S., Fox, M.S., and Leitman, D.C. (2006). Distinct roles of unliganded and liganded estrogen receptors in transcriptional repression. *Mol. Cell* *21*, 555–564.
- Demark-Wahnefried, W., Campbell, K.L., and Hayes, S.C. (2012). Weight management and its role in breast cancer rehabilitation. *Cancer* *118* (8 Suppl), 2277–2287.
- Dontu, G., Abdallah, W.M., Foley, J.M., Jackson, K.W., Clarke, M.F., Kawamura, M.J., and Wicha, M.S. (2003). In vitro propagation and transcriptional profiling of human mammary stem/progenitor cells. *Genes Dev.* *17*, 1253–1270.
- Eliassen, A.H., Missmer, S.A., Tworoger, S.S., Spiegelman, D., Barbieri, R.L., Dowsett, M., and Hankinson, S.E. (2006). Endogenous steroid hormone concentrations and risk of breast cancer among premenopausal women. *J. Natl. Cancer Inst.* *98*, 1406–1415.
- Engel, L.W., Young, N.A., Tralka, T.S., Lippman, M.E., O'Brien, S.J., and Joyce, M.J. (1978). Establishment and characterization of three new continuous cell lines derived from human breast carcinomas. *Cancer Res.* *38*, 3352–3364.
- Ferlay, J., Soerjomataram, I., Dikshit, R., Eser, S., Mathers, C., Rebelo, M., Parkin, D.M., Forman, D., and Bray, F. (2015). Cancer incidence and mortality worldwide: sources, methods and major patterns in GLOBOCAN 2012. *Int. J. Cancer* *136*, E359–E386.
- Finkelstein, E.A., Khavjou, O.A., Thompson, H., Trogdon, J.G., Pan, L., Sherry, B., and Dietz, W. (2012). Obesity and severe obesity forecasts through 2030. *Am. J. Prev. Med.* *42*, 563–570.
- Franco, H.L., Nagari, A., and Kraus, W.L. (2015). TNF α signaling exposes latent estrogen receptor binding sites to alter the breast cancer cell transcriptome. *Mol. Cell* *58*, 21–34.
- Frasor, J., Weaver, A., Pradhan, M., Dai, Y., Miller, L.D., Lin, C.Y., and Stanculescu, A. (2009). Positive cross-talk between estrogen receptor and NF- κ B in breast cancer. *Cancer Res.* *69*, 8918–8925.
- Frasor, J., El-Shennawy, L., Stender, J.D., and Kastrati, I. (2015). NF- κ B affects estrogen receptor expression and activity in breast cancer through multiple mechanisms. *Mol. Cell. Endocrinol.* *418*, 235–239.
- Ghisletti, S., Meda, C., Maggi, A., and Vegeto, E. (2005). 17 β -estradiol inhibits inflammatory gene expression by controlling NF- κ B intracellular localization. *Mol. Cell. Biol.* *25*, 2957–2968.
- Ginestier, C., Hur, M.H., Charafe-Jauffret, E., Monville, F., Dutcher, J., Brown, M., Jacquemier, J., Viens, P., Kleer, C.G., Liu, S., et al. (2007). ALDH1 is a marker of normal and malignant human mammary stem cells and a predictor of poor clinical outcome. *Cell Stem Cell* *1*, 555–567.
- Ginestier, C., Liu, S., Diebel, M.E., Korkaya, H., Luo, M., Brown, M., Wicinski, J., Cabaud, O., Charafe-Jauffret, E., Birnbaum, D., et al. (2010). CXCR1 blockade selectively targets human breast cancer stem cells in vitro and in xenografts. *J. Clin. Invest.* *120*, 485–497.
- Giraud, S.N., Caron, C.M., Pham-Dinh, D., Kitabgi, P., and Nicot, A.B. (2010). Estradiol inhibits ongoing autoimmune neuroinflammation and NF- κ B-dependent CCL2 expression in reactive astrocytes. *Proc. Natl. Acad. Sci. USA* *107*, 8416–8421.
- Grivnenkov, S.I., Greten, F.R., and Karin, M. (2010). Immunity, inflammation, and cancer. *Cell* *140*, 883–899.
- Grodin, J.M., Siiteri, P.K., and MacDonald, P.C. (1973). Source of estrogen production in postmenopausal women. *J. Clin. Endocrinol. Metab.* *36*, 207–214.
- Hilborn, E., Stål, O., and Jansson, A. (2017). Estrogen and androgen-converting enzymes 17 β -hydroxysteroid dehydrogenase and their involvement in cancer: with a special focus on 17 β -hydroxysteroid dehydrogenase type 1, 2, and breast cancer. *Oncotarget* *8*, 30552–30562.
- Hotamisligil, G.S., and Erbay, E. (2008). Nutrient sensing and inflammation in metabolic diseases. *Nat. Rev. Immunol.* *8*, 923–934.
- Howlander, N., Altekruse, S.F., Li, C.I., Chen, V.W., Clarke, C.A., Ries, L.A., and Cronin, K.A. (2014). US incidence of breast cancer subtypes defined by joint hormone receptor and HER2 status. *J. Natl. Cancer Inst.* *106*, dju055.
- Hoy, A.J., Balaban, S., and Saunders, D.N. (2017). Adipocyte-tumor cell metabolic crosstalk in breast cancer. *Trends Mol. Med.* *23*, 381–392.
- Iyengar, N.M., Morris, P.G., Zhou, X.K., Gucaip, A., Giri, D., Harbus, M.D., Falcone, D.J., Krasne, M.D., Vahdat, L.T., Subbaramaiah, K., et al. (2015). Menopause is a determinant of breast adipose inflammation. *Cancer Prev. Res. (Phila.)* *8*, 349–358.
- Kaaks, R., Rinaldi, S., Key, T.J., Berrino, F., Peeters, P.H., Biessy, C., Dossus, L., Lukanova, A., Bingham, S., Khaw, K.T., et al. (2005). Postmenopausal serum androgens, oestrogens and breast cancer risk: the European prospective investigation into cancer and nutrition. *Endocr. Relat. Cancer* *12*, 1071–1082.
- Kalaizidis, D., and Gilmore, T.D. (2005). Transcription factor cross-talk: the estrogen receptor and NF- κ B. *Trends Endocrinol. Metab.* *16*, 46–52.
- Kanneganti, T.D., and Dixit, V.D. (2012). Immunological complications of obesity. *Nat. Immunol.* *13*, 707–712.
- Key, T., Appleby, P., Barnes, I., and Reeves, G.; Endogenous Hormones and Breast Cancer Collaborative Group (2002). Endogenous sex hormones and breast cancer in postmenopausal women: reanalysis of nine prospective studies. *J. Natl. Cancer Inst.* *94*, 606–616.
- Key, T.J., Appleby, P.N., Reeves, G.K., Roddam, A., Dorgan, J.F., Longcope, C., Stanczyk, F.Z., Stephenson, H.E., Jr., Falk, R.T., Miller, R., et al.; Endogenous Hormones Breast Cancer Collaborative Group (2003). Body

mass index, serum sex hormones, and breast cancer risk in postmenopausal women. *J. Natl. Cancer Inst.* **95**, 1218–1226.

Key, T.J., Appleby, P.N., Reeves, G.K., Travis, R.C., Brinton, L.A., Helzlsouer, K.J., Dorgan, J.F., Gapstur, S.M., Gaudet, M.M., Kaaks, R., et al.; Endogenous Hormones and Breast Cancer Collaborative Group (2015). Steroid hormone measurements from different types of assays in relation to body mass index and breast cancer risk in postmenopausal women: reanalysis of eighteen prospective studies. *Steroids* **99** (Pt A), 49–55.

Knazek, R.A., Lippmann, M.E., and Chopra, H.C. (1977). Formation of solid human mammary carcinoma in vitro. *J. Natl. Cancer Inst.* **58**, 419–422.

Ligibel, J.A., Alfano, C.M., Courneya, K.S., Demark-Wahnefried, W., Burger, R.A., Chlebowski, R.T., Fabian, C.J., Gucalp, A., Hershman, D.L., Hudson, M.M., et al. (2014). American Society of Clinical Oncology position statement on obesity and cancer. *J. Clin. Oncol.* **32**, 3568–3574.

Ling, J., and Kumar, R. (2012). Crosstalk between NFκB and glucocorticoid signaling: a potential target of breast cancer therapy. *Cancer Lett.* **322**, 119–126.

Lippman, M. (1976). Steroid hormone receptors in human malignancy. *Life Sci.* **78**, 143–152.

Lippman, M.E., and Allegra, J.C. (1978). Current concepts in cancer. Receptors in breast cancer. *N. Engl. J. Med.* **299**, 930–933.

Lippman, M., Bolan, G., and Huff, K. (1976). The effects of estrogens and antiestrogens on hormone-responsive human breast cancer in long-term tissue culture. *Cancer Res.* **36**, 4595–4601.

Lippman, M., Monaco, M.E., and Bolan, G. (1977). Effects of estrone, estradiol, and estril on hormone-responsive human breast cancer in long-term tissue culture. *Cancer Res.* **37**, 1901–1907.

Lønning, P.E., Haynes, B.P., Straume, A.H., Dunbier, A., Helle, H., Knappskog, S., and Dowsett, M. (2011). Exploring breast cancer estrogen disposition: the basis for endocrine manipulation. *Clin. Cancer Res.* **17**, 4948–4958.

Ma, C.X., Reinert, T., Chmielewska, I., and Ellis, M.J. (2015). Mechanisms of aromatase inhibitor resistance. *Nat. Rev. Cancer* **15**, 261–275.

MacDonald, P.C., Edman, C.D., Hemsell, D.L., Porter, J.C., and Siiteri, P.K. (1978). Effect of obesity on conversion of plasma androstenedione to estrone in postmenopausal women with and without endometrial cancer. *Am. J. Obstet. Gynecol.* **130**, 448–455.

Medzhitov, R. (2008). Origin and physiological roles of inflammation. *Nature* **454**, 428–435.

Miyoshi, Y., Tanji, Y., Taguchi, T., Tamaki, Y., and Noguchi, S. (2003). Association of serum estrone levels with estrogen receptor-positive breast cancer risk in postmenopausal Japanese women. *Clin. Cancer Res.* **9**, 2229–2233.

Morris, P.G., Hudis, C.A., Giri, D., Morrow, M., Falcone, D.J., Zhou, X.K., Du, B., Brogi, E., Crawford, C.B., Kopelovich, L., et al. (2011). Inflammation and increased aromatase expression occur in the breast tissue of obese women with breast cancer. *Cancer Prev. Res. (Phila.)* **4**, 1021–1029.

Mukherjee, K., Syed, V., and Ho, S.M. (2005). Estrogen-induced loss of progesterone receptor expression in normal and malignant ovarian surface epithelial cells. *Oncogene* **24**, 4388–4400.

Munsell, M.F., Sprague, B.L., Berry, D.A., Chisholm, G., and Trentham-Dietz, A. (2014). Body mass index and breast cancer risk according to postmenopausal estrogen-progestin use and hormone receptor status. *Epidemiol. Rev.* **36**, 114–136.

Nettles, K.W., Gil, G., Nowak, J., Métivier, R., Sharma, V.B., and Greene, G.L. (2008). CBP is a dosage-dependent regulator of nuclear factor-κB suppression by the estrogen receptor. *Mol. Endocrinol.* **22**, 263–272.

Nichols, H.B., Trentham-Dietz, A., Egan, K.M., Titus-Ernstoff, L., Holmes, M.D., Bersch, A.J., Holick, C.N., Hampton, J.M., Stampfer, M.J., Willett, W.C., and Newcomb, P.A. (2009). Body mass index before and after breast cancer diagnosis: associations with all-cause, breast cancer, and cardiovascular disease mortality. *Cancer Epidemiol. Biomarkers Prev.* **18**, 1403–1409.

Nicolini, A., Carpi, A., and Rossi, G. (2006). Cytokines in breast cancer. *Cytokine Growth Factor Rev.* **17**, 325–337.

Nimrod, A., and Ryan, K.J. (1975). Aromatization of androgens by human abdominal and breast fat tissue. *J. Clin. Endocrinol. Metab.* **40**, 367–372.

Nwachukwu, J.C., Srinivasan, S., Bruno, N.E., Parent, A.A., Hughes, T.S., Pollock, J.A., Gijshi, O., Cavett, V., Nowak, J., Garcia-Ordóñez, R.D., et al. (2014). Resveratrol modulates the inflammatory response via an estrogen receptor-signal integration network. *eLife* **3**, e02057.

Pasqualini, J.R., Chetrite, G., Blacker, C., Feinstein, M.C., Delalonde, L., Talbi, M., and Maloche, C. (1996). Concentrations of estrone, estradiol, and estrone sulfate and evaluation of sulfatase and aromatase activities in pre- and postmenopausal breast cancer patients. *J. Clin. Endocrinol. Metab.* **81**, 1460–1464.

Pfeilschifter, J., Köditz, R., Pfohl, M., and Schatz, H. (2002). Changes in proinflammatory cytokine activity after menopause. *Endocr. Rev.* **23**, 90–119.

Picon-Ruiz, M., Pan, C., Drews-Elger, K., Jang, K., Besser, A.H., Zhao, D., Morata-Tarifa, C., Kim, M., Ince, T.A., Azzam, D.J., et al. (2016). Interactions between adipocytes and breast cancer cells stimulate cytokine production and drive Src/Sox2/miR-302b-mediated malignant progression. *Cancer Res.* **76**, 491–504.

Picon-Ruiz, M., Morata-Tarifa, C., Valle-Goffin, J.J., Friedman, E.R., and Slingerland, J.M. (2017). Obesity and adverse breast cancer risk and outcome: mechanistic insights and strategies for intervention. *CA Cancer J. Clin.* **67**, 378–397.

Poirier, D. (2015). Recent patents on new steroid agents targeting the steroidogenesis for endocrine cancer treatments. *Recent Pat. Endocr. Metab. Immune Drug Discov.* **9**, 15–23.

Pradhan, M., Bembinsten, L.A., Baumgarten, S.C., and Frasier, J. (2010). Proinflammatory cytokines enhance estrogen-dependent expression of the multidrug transporter gene ABCG2 through estrogen receptor and NFκB cooperativity at adjacent response elements. *J. Biol. Chem.* **285**, 31100–31106.

Purohit, A., and Reed, M.J. (2002). Regulation of estrogen synthesis in postmenopausal women. *Steroids* **67**, 979–983.

Purohit, A., Newman, S.P., and Reed, M.J. (2002). The role of cytokines in regulating estrogen synthesis: implications for the etiology of breast cancer. *Breast Cancer Res.* **4**, 65–69.

Quail, D.F., and Dannenberg, A.J. (2019). The obese adipose tissue microenvironment in cancer development and progression. *Nat. Rev. Endocrinol.* **15**, 139–154.

Renehan, A.G., Zwahlen, M., and Egger, M. (2015). Adiposity and cancer risk: new mechanistic insights from epidemiology. *Nat. Rev. Cancer* **15**, 484–498.

Romieu-Mourez, R., Kim, D.W., Shin, S.M., Demicco, E.G., Landesman-Bollag, E., Seldin, D.C., Cardiff, R.D., and Sonenshein, G.E. (2003). Mouse mammary tumor virus c-rel transgenic mice develop mammary tumors. *Mol. Cell. Biol.* **23**, 5738–5754.

Sandhu, C., Garbe, J., Bhattacharya, N., Dakis, J., Pan, C.H., Yaswen, P., Koh, J., Slingerland, J.M., and Stampfer, M.R. (1997). Transforming growth factor beta stabilizes p15INK4B protein, increases p15INK4B-cdk4 complexes, and inhibits cyclin D1-cdk4 association in human mammary epithelial cells. *Mol. Cell. Biol.* **17**, 2458–2467.

Sansone, P., Storci, G., Tavolari, S., Guarnieri, T., Giovannini, C., Taffurelli, M., Ceccarelli, C., Santini, D., Paterini, P., Marcu, K.B., et al. (2007). IL-6 triggers malignant features in mammospheres from human ductal breast carcinoma and normal mammary gland. *J. Clin. Invest.* **117**, 3988–4002.

Santen, R.J., Brodie, H., Simpson, E.R., Siiteri, P.K., and Brodie, A. (2009). History of aromatase: saga of an important biological mediator and therapeutic target. *Endocr. Rev.* **30**, 343–375.

Sas, L., Lardon, F., Vermeulen, P.B., Hauspy, J., Van Dam, P., Pauwels, P., Dirix, L.Y., and Van Laere, S.J. (2012). The interaction between ER and NFκB in resistance to endocrine therapy. *Breast Cancer Res.* **14**, 212.

Sasson, S., and Notides, A.C. (1983). Estril and estrone interaction with the estrogen receptor. I. Temperature-induced modulation of the cooperative binding of [3H]estril and [3H]estrone to the estrogen receptor. *J. Biol. Chem.* **258**, 8113–8117.

- Schäffler, A., and Schölmerich, J. (2010). Innate immunity and adipose tissue biology. *Trends Immunol.* *31*, 228–235.
- Schindler, A.E., Ebert, A., and Friedrich, E. (1972). Conversion of androstenedione to estrone by human tissue. *J. Clin. Endocrinol. Metab.* *35*, 627–630.
- Siiteri, P.K. (1982). Review of studies on estrogen biosynthesis in the human. *Cancer Res.* *42* (8 Suppl), 3269s–3273s.
- Siiteri, P.K., and MacDonald, P.C. (1973). Role of extraglandular estrogen in human endocrinology. In *Handbook of Physiology*, R.O. Greep and E.B. Astwood, eds. (American Physiologic Society), pp. 615–629.
- Simpkins, F., Hevia-Paez, P., Sun, J., Ullmer, W., Gilbert, C.A., da Silva, T., Pedram, A., Levin, E.R., Reis, I.M., Rabinovich, B., et al. (2012). Src inhibition with saracatinib reverses fulvestrant resistance in ER-positive ovarian cancer models in vitro and in vivo. *Clin. Cancer Res.* *18*, 5911–5923.
- Soria, G., and Ben-Baruch, A. (2008). The inflammatory chemokines CCL2 and CCL5 in breast cancer. *Cancer Lett.* *267*, 271–285.
- Stein, B., and Yang, M.X. (1995). Repression of the interleukin-6 promoter by estrogen receptor is mediated by NF-kappa B and C/EBP beta. *Mol. Cell. Biol.* *15*, 4971–4979.
- Stender, J.D., Nwachukwu, J.C., Kastrati, I., Kim, Y., Strid, T., Yakir, M., Srinivasan, S., Nowak, J., Izard, T., Rangarajan, E.S., et al. (2017). Structural and molecular mechanisms of cytokine-mediated endocrine resistance in human breast cancer cells. *Mol. Cell* *65*, 1122–1135.e5.
- Strobl, J.S., and Lippman, M.E. (1979). Prolonged retention of estradiol by human breast cancer cells in tissue culture. *Cancer Res.* *39*, 3319–3327.
- Subramanian, A., Tamayo, P., Mootha, V.K., Mukherjee, S., Ebert, B.L., Gillette, M.A., Paulovich, A., Pomeroy, S.L., Golub, T.R., Lander, E.S., and Mesirov, J.P. (2005). Gene set enrichment analysis: a knowledge-based approach for interpreting genome-wide expression profiles. *Proc. Natl. Acad. Sci. USA* *102*, 15545–15550.
- Suzuki, R., Orsini, N., Saji, S., Key, T.J., and Wolk, A. (2009). Body weight and incidence of breast cancer defined by estrogen and progesterone receptor status—a meta-analysis. *Int. J. Cancer* *124*, 698–712.
- Tornatore, L., Thotakura, A.K., Bennett, J., Moretti, M., and Franzoso, G. (2012). The nuclear factor kappa B signaling pathway: integrating metabolism with inflammation. *Trends Cell Biol.* *22*, 557–566.
- Toyama, E.Q., Herzig, S., Courchet, J., Lewis, T.L., Jr., Losón, O.C., Hellberg, K., Young, N.P., Chen, H., Polleux, F., Chan, D.C., and Shaw, R.J. (2016). Metabolism. AMP-activated protein kinase mediates mitochondrial fission in response to energy stress. *Science* *351*, 275–281.
- Tsuyada, A., Chow, A., Wu, J., Somlo, G., Chu, P., Loera, S., Luu, T., Li, A.X., Wu, X., Ye, W., et al. (2012). CCL2 mediates cross-talk between cancer cells and stromal fibroblasts that regulates breast cancer stem cells. *Cancer Res.* *72*, 2768–2779.
- Vallabhapurapu, S., and Karin, M. (2009). Regulation and function of NF-kappaB transcription factors in the immune system. *Annu. Rev. Immunol.* *27*, 693–733.
- van Landeghem, A.A., Poortman, J., Nabuurs, M., and Thijssen, J.H. (1985). Endogenous concentration and subcellular distribution of estrogens in normal and malignant human breast tissue. *Cancer Res.* *45*, 2900–2906.
- Vance, V., Mourtzakis, M., McCargar, L., and Hanning, R. (2011). Weight gain in breast cancer survivors: prevalence, pattern and health consequences. *Obes. Rev.* *12*, 282–294.
- Vincze, B., Kapuvári, B., Udvarhelyi, N., Horváth, Z., Mátrai, Z., Czeyda-Pommersheim, F., Kóhalmy, K., Kovács, J., Boldizsár, M., Láng, I., and Kásler, M. (2015). Serum estrone concentration, estrone sulfate/estrone ratio and BMI are associated with human epidermal growth factor receptor 2 and progesterone receptor status in postmenopausal primary breast cancer patients suffering invasive ductal carcinoma. *Springerplus* *4*, 387.
- Vona-Davis, L., and Rose, D.P. (2009). Angiogenesis, adipokines and breast cancer. *Cytokine Growth Factor Rev.* *20*, 193–201.
- Wang, X., Simpson, E.R., and Brown, K.A. (2015). Aromatase overexpression in dysfunctional adipose tissue links obesity to postmenopausal breast cancer. *J. Steroid Biochem. Mol. Biol.* *153*, 35–44.
- Ward, Z.J., Bleich, S.N., Cradock, A.L., Barrett, J.L., Giles, C.M., Flax, C., Long, M.W., and Gortmaker, S.L. (2019). Projected U.S. state-level prevalence of adult obesity and severe obesity. *N. Engl. J. Med.* *381*, 2440–2450.
- Waugh, D.J., and Wilson, C. (2008). The interleukin-8 pathway in cancer. *Clin. Cancer Res.* *14*, 6735–6741.
- Yu, H., Shu, X.O., Shi, R., Dai, Q., Jin, F., Gao, Y.T., Li, B.D., and Zheng, W. (2003). Plasma sex steroid hormones and breast cancer risk in Chinese women. *Int. J. Cancer* *105*, 92–97.

STAR★METHODS

KEY RESOURCES TABLE

REAGENT or RESOURCE	SOURCE	IDENTIFIER
Antibodies		
Anti-Aromatase (D5Q2Y) Rabbit mAb	Cell Signaling Technology	Cat#14528; RRID: AB_2630344
Anti-GAPDH (14C10) Rabbit mAb	Cell Signaling Technology	Cat#2118; RRID: AB_561053
Anti-Sox2 (D6D9) XP Rabbit mAb	Cell Signaling Technology	Cat#3579S; RRID: AB_2195767
Anti-OCT-4 Rabbit polyclonal Ab	Cell Signaling Technology	Cat#2750; RRID: AB_823583
Anti-KLF4 Rabbit polyclonal Ab	Cell Signaling Technology	Cat#4038; RRID: AB_2265207
Anti-HSD17B14 antibody Ab	Abcam	Cat # ab87011
Anti-ER alpha (F-10) Mouse mAb	Santa Cruz	Cat#SC8002; RRID: AB_627558
Anti -SRC3 antibody Rabbit polyclonal Ab	Bethyl Laboratories	Cat# A300-348-A
Anti -CBP-antibody Mouse Monoclonal Ab	Santa Cruz	Cat#SC-7300
Acetyl-CBP (Lys1535)/p300 (Lys1499) Antibody	Cell Signaling	Cat #4771S
Anti-H3K27Ac(Mouse mAb) Antibody	Active Motif	Cat#39685
Anti-Ki67 Rabbit polyclonal	Abcam	Cat#ab15580
Normal mouse IgG	Santa Cruz	Cat#SC-2025
Normal Rabbit IgG	Santa Cruz	Cat# SC-2027
Anti-β-Actin (AC-15) Mouse mAb	Sigma	Cat#A1978; RRID: AB_476692
NFκB p65 (C22B4) Rabbit mAb	Cell Signaling Technology	Cat#4764; RRID: AB_823578
Anti-β-tubulin (9F3) Rabbit mAb	Cell Signaling Technology	Cat#2128; RRID: AB_823664
Anti-Lamin B2 (D8P3U) Rabbit mAb	Cell Signaling Technology	Cat#12255; RRID: AB-12255S
Anti-Phospho NF-κB (p65) Ser 536 Rabbit mAb	Cell Signaling Technology	Cat#3033; RRID: AB_331284
Anti-Mouse IgG (H+L), HRP Conjugate	Promega	Cat#W4021; RRID: AB_430834
Anti-Rabbit IgG (H+L), HRP Conjugate	Promega	Cat#W4011; RRID: AB_430833
Bacterial and Virus Strains		
One Shot MAX Efficiency DH5α-T1R Competent Cells	Invitrogen	Cat#12297-016
pGL4.32[luc2P/NF-κB-RE/Hygro]	Promega	Cat#E8491
pGL4 [Luc2P/ERE/Hygro] vector	This paper	N/A
pLenti.PGK.blast-Renilla_Luciferase	Addgene	Cat# 74444
Biological Samples		
Female Adult Human Abdominal Adipose Tissue	University of Miami	N/A
Female Adult Human Breast Adipose Tissue	University of Miami	N/A
Chemicals, Peptides, and Recombinant Proteins		
Collagenase from Clostridium histolyticum Type IA	Sigma-Aldrich	Cat#C9891
TRIzol Reagent	Invitrogen	Cat#10296-028
iQ SYBR Green Supermix	Bio-Rad	Cat#170-8886
Hydrocortisone	StemCell Technologies	Cat#7925
Heparin Solution	StemCell Technologies	Cat#7980
Insulin, human recombinant, zinc solution	Thermo Fisher Scientific	Cat#12585014
B27 Supplement (50X), serum free	Thermo Fisher Scientific	Cat#17504044
Recombinant Human EGF Protein, CF	R&D Systems	Cat#236-EG
FGF-Basic (AA 10-155) Recombinant Human	Thermo Fisher Scientific	Cat# PHG0026
RIPA Buffer	Cell Signaling	Cat#9806
PhosphataseArrest Phosphatase Inhibitor Cocktail	G-Biosciences	Cat#786-450
ProteaseArrest Protease Inhibitor Cocktail	G-Biosciences	Cat#786-331
Pierce ECL Western Blotting Substrate	Thermo Scientific	Cat#32106
Letrozole	Sigma-Aldrich	Cat#L6545

(Continued on next page)

Continued

REAGENT or RESOURCE	SOURCE	IDENTIFIER
B-Estradiol	Sigma-Aldrich	Cat#E8875
Estrone	Sigma-Aldrich	Cat# E9750
BAY 11-7082	Sigma-Aldrich	Cat# B5556
TNF- α Human	Sigma-Aldrich	Cat# SRP3177
Luciferin	PERKINELMER	Cat# 770504
Lipofectamine 3000 Reagent	Invitrogen	Cat# L3000015
Fulvestrant	Selleckchem	Cat# S1191
Puromycin	GIBCO Life Technology	Cat# A11113803
Critical Commercial Assays		
iScript cDNA Synthesis Kit	Bio-Rad	Cat#1708891
Truseq standard Total RNA Library Prep	Illumina, San Diego	N/A
ALDEFLUOR kit	Stem Cell Technologies	Cat#01700
Estradiol ELISA Kit (Competitive EIA)	LifeSpan BioSciences	Cat#LS-F5297
Estrone ELISA Kit (Competitive EIA)	LifeSpan BioSciences	Cat#LS-F10566
Cytokine/Chemokine/Growth Factor 45-Plex Human ProcartaPlex Panel 1	Invitrogen	Cat#EPX450-12171-901
RNeasy Lipid Tissue Kit	QIAGEN	Cat#74804
NE-PER Nuclear and cytoplasmic extraction reagents	Thermo Fisher Scientific	Cat#78835
Dual-Luciferase Reporter Assay System	Promega	Cat#E1960
Proteome Profiler Human Cytokine Array Kit	R&D	Cat# ARY005B
NEBNext Ultra II RNA Library Prep Kit for Illumina	Illumina	Cat # E7765S
Kappa Pure Beads KR1245-V3.16	Kapa Biosystem	KK8000
Deposited Data		
RNA Seq	This Paper	GEO: GSE132913
Kaplan Meier(KM) Plotter	KM Plotter	https://kmpplot.com/analysis/
UALCAN	UAB	http://ualcan.path.uab.edu/index.html
Experimental Models: Cell Lines		
Human: MDA-MB-231	ATCC	HTB-26
Human: SUM149	Steven Ethiers	CVCL_3422
Human: SUM159	Steven Ethiers	CVCL_5423
Human: SUM1315	Steven Ethiers	CVCL_5589
Human: MCF7	ATCC	HTB-22
Human: T47D	ATCC	HTB-133
Human: MDA-MB-361	ATCC	HTB-27
Human: MCF12A	ATCC	CRL-10782
Mouse: E0771 cells	CH3 BioSystems	SkU:940001
Experimental Models: Organisms/Strains		
Mouse: NF- κ B-luc: B10.Cg-H2 ^k Tg(NFkB/Fos-luc)26Rinc/J	The Jackson Laboratory	JAX: 006100
000664 - C57BL/6J Ovariectomized	The Jackson Laboratory	JAX –000664
NOD.CB17-Prkdc < scid > /J HOM Homozygous for Prkdc < scid > ovariectomized	The Jackson Laboratory	JAX- 001303
NOD.Cg-Prkdc < scid > Il2rg < tm1Wjl > /SzJ M01 Homozygous for Prkdc < scid > , Homozygous for Il2rg < tm1Wjl > ovariectomized	The Jackson Laboratory	JAX- 005557
Oligonucleotides		
QPCR PRIMER		
Primer PCR: GAPDH Forward: 5'-ATCAAGTGGGGCGATGCTG-3'	This paper	N/A

(Continued on next page)

Continued

REAGENT or RESOURCE	SOURCE	IDENTIFIER
Primer PCR: GAPDH Reverse: 5'-ACCCATGACGAACATGGGG-3'	This paper	N/A
Primer PCR: CCl2 Forward: 5'-AAGAAGCTGTGATCTTCAAGAC-3'	This paper	N/A
Primer PCR: CCl2 Reverse: 5'-CCATGGAATCCTGAACCCA-3'	This paper	N/A
Primer PCR IL6 Forward: 5'-GATTC AATGAGGAGACTTGCC-3'	This paper	N/A
Primer PCR IL6 Reverse: 5'-TGTTCTGGAGGTACTCTAGGT-3'	This paper	N/A
Primer PCR IL8 Forward: 5'-TGCCAAGGAGTGCTAAAG-3'	This Paper	N/A
Primer PCR IL8 Reverse: 5'-AATTTCTGTGTTGGCGCAGT-3'	This Paper	N/A
Primer PCR SOX2 Forward: 5'-CGAGTAGGACATGCTGTAGGT-3'	This Paper	N/A
Primer PCR SOX2 Reverse: 5'-TGGACAGTTACGCGCACAT-3'	This Paper	N/A
Primer PCR NANOG Forward: 5'-GCTTTGAAGCATCCGACTG-3'	This Paper	N/A
Primer PCR NANOG Reverse: 5'-GATAGTTTTCTTCAGGCCACA-3'	This Paper	N/A
Primer PCR KLF4 Forward: 5'-CCCACACTTGTGATTACGC-3'	This Paper	N/A
Primer PCR KLF4 Reverse: 5'-GGTAAGGTTTCTCACCTGTG-3'	This Paper	N/A
Primer PCR OCT4 Forward: 5'-GAGAAGGATGTGGTCCGAG-3'	This Paper	N/A
Primer PCR OCT4 Reverse: 5'-TCCTCTCGTTGTGCATAGTC-3'	This Paper	N/A
Primer PCR HSD17B14 Forward: 5'-TGCGACAAGGATGAGTCTG-3'	This Paper	N/A
Primer PCR HSD17B14 Reverse: 5'-CTGAGTCACATCACAGAGGA-3'	This Paper	N/A
Primer PCR cMYC Forward: 5'-GAGTCTGGATCACCTTCTGCTG-3'	This Paper	N/A
Primer PCR cMYC Reverse: 5'-AGGATAGTCCTTCCGAGTGGAG-3'	This Paper	N/A
Primer PCR CD44 Forward: 5'-CTGCCGCTTGCAGGTGTA-3'	This Paper	N/A
Primer PCR CD44 Reverse: 5'-CATTGTGGCAAGGTGCTATT-3'	This Paper	N/A
Primer PCR TLR2 Forward: 5'-ATCCTCCAATCAGGCTTCTCT-3'	This paper	N/A
Primer PCR TLR2 Reverse: 5'-GGACAGGTCAAGGCTTTTACA-3'	This Paper	N/A
Primer PCR NFKB1 Forward: 5'-AACAGAGAGGATTCGTTCCG-3'	This paper	N/A
Primer PCR NFKB1 Reverse: 5'-TTTGACCTGAGGGTAAGACTTCT-3'	This Paper	N/A
Primer PCR Rela Forward: 5'-ATGTGGAGATCATTGAGCAGC-3'	This Paper	N/A
Primer PCR Rela Reverse: 5'-CCTGGTCTGTGTAGCCATT-3'	This Paper	N/A

(Continued on next page)

Continued

REAGENT or RESOURCE	SOURCE	IDENTIFIER
Primer PCR PTPN1 Forward: 5'-GCAGATCGACAAGTCCGGG-3'	This Paper	N/A
Primer PCR PTPN1 Reverse: 5'-GCCACTCTACATGGGAAGTCAC-3'	This Paper	N/A
Primer PCR PAK4 Forward: 5'-GGACATCAAGAGCGACTCGAT-3'	This Paper	N/A
Primer PCR PAK4 Reverse: 5'-CGACCAGCGACTTCCTTCG-3'	This Paper	N/A
Primer PCR Rab19 Forward: 5'-GTGCAGCATTCAAGTCTGGA-3'	This Paper	N/A
Primer PCR Rab19 Reverse: 5'-CAAGGGAACGCACGGTAAAGT-3'	This Paper	N/A
Primer PCR ALDH16A1 Forward: 5'-CACCTCGCTGGAGTACGGA-3'	This Paper	N/A
Primer PCR ALDH16A1 Reverse: 5'-CCATTCACATAGTGGCCCAAG-3'	This Paper	N/A
Primer PCR CD160 Forward: 5'-GCTGAGGGGTTTGTAGTGT -3'	This Paper	N/A
Primer PCR CD160 Reverse: 5'-GTGTGACTTGGCTTATGGTGA -3'	This Paper	N/A
Primer PCR CSTL1 Forward: 5'-ATGGGGATCGGATGCTGGA-3'	This Paper	N/A
Primer PCR CSTL1 Reverse: 5'-TGCTCGTGCATTCTCTTGC -3'	This Paper	N/A
Primer PCR ZNF626 Forward: 5'-TTCAAACGGACAAAAGAGAGGAC-3'	This Paper	N/A
Primer PCR ZNF626 Reverse: 5'-GGCTACAAGAGTGGTTAAAGGC-3'	This Paper	N/A
Primer 'Forward Primer PS2: 5'-CCCGTGAAAGACAGAATTGT-3'	This Paper	N/A
Primer Reverse Primer PS2: 5'-GGTGTCTCGAAACAGCAG-3'	This Paper	N/A
Primer Forward Primer GREB1: 5'-CTGTACCACAGACGGGTTTTG-3'	This Paper	N/A
Primer Reverse Primer GREB1: 5'-TTCCGTGAAGTAACAGAAGCC-3'	This Paper	N/A
Primer Forward Primer PGR: 5'-ACCCGCCCTATCTCACTACC-3'	This Paper	N/A
Primer Reverse Primer PGR: 5'-AGGACACCATAATGACAGCCT-3'	This Paper	N/A
CHIP Primer		
Primer PCR CCL2 Forward: 5'-CCAGCCAAATGCATTCTCTT-3'	This Paper	N/A
Primer PCR CCL2 Reverse: 5'-GCTGGCGTGAGAGAAGTGAG-3'	This Paper	N/A
Primer PCR IL6 Forward: 5'-TGGCAAAAAGGAGTCACACA-3'	This Paper	N/A
Primer PCR IL6 Reverse: 5'-CTGTGAGCGGCTGTTGTAGA-3'	This Paper	N/A
Neg control CCL2 F: 5'-TCTTTCCAGAGAGCTCACTTTT-3'	This Paper	N/A
Neg Control CCL2 R: 5'-CTCCTCTTGGTGAATAATGCTTTC-3'	This Paper	N/A

(Continued on next page)

Continued

REAGENT or RESOURCE	SOURCE	IDENTIFIER
Neg Control IL6 F: 5'- CGTCCGTAGTTTCCTTAGCTT- 3'	This Paper	N/A
Neg Control IL6 R: 5'- ACTTGGTTCAGGGCAGAAAAG- 3'	This Paper	N/A
Primer PCR PS2 Forward: 5'- CTAGACGGAATGGGCTTCAT- 3'	This Paper	N/A
Primer PCR PS2 Reverse: 5' - CTCCCGCCAGGGTAAATACT -3'	This Paper	N/A
Primer PCR GREB1 Forward: 5'- GTGGCAACTGGGTCATTCTGA- 3'	This Paper	N/A
Primer PCR GREB1 Reverse: 5'- CGACCCACAGAAATGAAAAGG -3'.	This Paper	N/A
Recombinant DNA		
ORF expression clone for human HSD17B14 (NM_016246.2))	Genecopoeia	EX-U0801-Lv224
17β-HSD14 CRISPR/Cas9 KO Plasmid (h)	Santa Cruz	Sc-412138
Software and Algorithms		
Adobe Illustrator	Adobe Systems, San Jose, CA	https://www.adobe.com/ca/products/illustrator.html ; RRID: SCR_010279
FlowJo software V10	FlowJo, LLC	https://www.flowjo.com/
Other		
10% Kcal from fat rodent food (LFD)	ENVIGO	Cat#TD.94048
60% Kcal from fat rodent food (HFD)	ENVIGO	Cat#TD.06414
Estradiol 0.36mg/90 day pellet	Innovative Research of America	Cat#NE-121
Estrone 0.36mg/90 day pellet	Innovative Research of America	Cat#NE-111
Estradiol 0.1mg/90 day pellet	Innovative Research of America	Cat#NE-121
Estrone 0.1mg/ pellet 90 day	Innovative Research of America	Cat#NE-111
Placebo 0.1mg/ pellet 90 day	Innovative Research of America	Cat# NC-111

RESOURCE AVAILABILITY

Lead Contact

Further information and requests for resources and reagents should be directed to the Lead Contact, Slingerland J (jslingerland@med.miami.edu).

Materials Availability

All unique/stable reagents generated in this study are available from the Lead Contact with a complete Materials Transfer Agreement.

Data and Code Availability

The RNA seq data generated during this study are available at Gene Expression Omnibus (GEO: GSE132913).

EXPERIMENTAL MODEL AND SUBJECT DETAILS

Human Subjects

This study conformed to the principles outlined in the Declaration of Helsinki. All human subjects provided written informed consent prior to donation of adipose tissue samples under an Institutional Review Board reviewed and exempted protocol. Samples obtained from human subjects were de-identified waste material from reduction mammoplasty, lumpectomy or mastectomy surgeries performed at the University of Miami Hospital. Donor BMI, age, menopausal status, and, if applicable, any cancer treatment received prior to surgery was recorded.

Mouse Models

All animal experiments and procedures were performed according to protocols approved by the Institutional Animal Care and Use Committee at University of Miami (Protocol # 16-084 LF rev). NFκB-luc (B10. Cg-H2^k Tg(NFκB/Fos-luc)26Rinc/J) mice were

purchased from the Jackson Laboratory and then bred in our facility. NOD-SICD mice were used for xenograft assays testing effects of steroids and HSD17B14 expression on tumor latency and growth (see below). NSG (NOD.Cg-Prkdcscid Il2rgtm1Wjl/SzJ) mice were used for limiting dilution assays of T-ISC with the MCF7 model. 000664 - C57BL/6J mice were used for syngeneic tumor implantation with the E0771 cell line (details below). Mice were housed in micro-isolator cages, with standard 12 h light/darkness cycle, ambient temperature 23°C and were provided standard rodent diet, unless otherwise indicated, and water *ad libitum*. Unless otherwise indicated, estrogen pellets containing either E1 or E2 at 0.1 mg/90 day were used for hormone supplementation. All controls not receiving estrogen supplements had control pellets containing no estrogen inserted. All mice were ovariectomized at 6 weeks of age.

Adipocyte, SVF and hASC Isolation from Fat Tissue

A total of 3 abdominal and 74 breast fat samples were used in this work. Adipose tissues from abdominal or mammary fat were washed 4X with PBS, digested with collagenase 1A 1 g/L in HANK'S solution supplemented with 1% BSA for 30 min at 37°C, and centrifuged at 1500 rpm for 5 min (Figure S1A). Floating mature adipocytes and pelleted SVF were separated, washed 3X with PBS and filtered using a 100 μm or 70 μm diameter membrane, respectively. hASC were obtained by seeding the SVF in 75 cm² culture flasks in DMEM medium supplemented with 10% FBS and 1% P/S. After 3 passages hASC were characterized by flow cytometry as in (Picon-Ruiz et al., 2016). Adipocytes were used immediately after isolation. hASC were used between passages 3-10.

Cell Culture

MDA-MB-231, MCF7, T47D, MCF12A and 293T and MDA-MB-361 were purchased from ATCC and grown per ATCC protocols. SUM149, SUM159, SUM1315 were provided by Steven Ethiers (Medical University of South Carolina) and grown as described in <http://sumlineknowledgebase.com/>. Isolated hASC and mature adipocytes were cultured alone or co-cultured for 6 days with the specified breast cancer cell lines using the corresponding cell line medium, unless specified otherwise. Fresh medium was added to the cultures at days 2 and 4 without discarding the old media in order to preserve the secretome. For experiments involving *in vitro* estrogen treatment, cancer lines were estrogen deprived by culture in phenol red-free medium supplemented with 5% charcoal stripped FBS for 48-72 h. Estrogen stimulation used media containing 5% cFBS together with either DMSO vehicle only, or E2 or E1 added at 10 nM, unless otherwise indicated for titration experiments. Where indicated, fulvestrant (ICI182,780) was used *in vitro* at 10 nM. Fulvestrant alone controls were completed for all experiments but not shown unless they changed expression versus control. Negative data are reported in the results section. CCL2, IL6 and TNF α were added to tissue culture media each at 10 ng/mL.

METHOD DETAILS

Cytokine Assays

Cytokine arrays were performed on the supernatant of abdominal and breast adipocytes after 48 h of culture *in vitro*. Media were collected from triplicate biologic assays and cytokine concentrations assayed by Cytokine/Chemokine/Growth Factor 45-Plex Human ProcartaPlex Panel 1 (Invitrogen) using Luminex Bio-Plex 200 plate reader (Bio-Rad). This same methodology was used for assays of mouse serum cytokines in Figures 4 and 6. Mouse serum was collected from at least 3 representative mice per group and cytokine concentrations were assayed with the Cytokine/Chemokine/Growth Factor 45-Plex Mouse ProcartaPlex Panel 1 (Invitrogen) using Luminex Bio-Plex 200 plate reader (Bio-Rad).

Assays of cytokine secretion into media of control and *HSD17B14* overexpressing lines used the Human Cytokine Array Kit from R&D Systems (Minneapolis, MN) to evaluate a panel of 36 proinflammatory cytokines per manufacturer's instructions. Media was collected 5 days after plating and triplicate repeats pooled and evaluated in a single array. Each cytokine level on the membrane was normalized to the intensity of positive control spots. Signal intensity which is graphed in arbitrary units versus control expressed as one.

Quantitative RT-PCR (qPCR)

Total RNA was isolated using Trizol (Invitrogen) or RNeasy Lipid Tissue Kit (QIAGEN) for adipocytes. cDNA was synthesized from the isolated RNA using iScript cDNA synthesis kit (Bio-Rad). qPCR was performed with a LightCycler 480 Instrument II (Roche) using iQ SYBR Green Supermix (Bio-Rad). All qPCR analyses were performed as both biologic and technical triplicate repeats. Primer sequences are shown in [Key Resources Table](#).

Aldehyde Dehydrogenase Activity by ALDEFLUOR Assay

ALDEFLUOR kit (Stem Cell Technologies) was used to detect ALDH enzymatic activity. Briefly, single cell suspensions were prepared at 10⁶ cells/mL in ALDEFLUOR assay buffer. ALDH activity was assayed by adding 5 μL Aldefluor reagent per 10⁶ cells followed by incubation at 37°C for 45 min and flow cytometry analysis. For each sample, the specific ALDH inhibitor diethylaminobenzaldehyde (DEAB) was used as a negative control for gating on flow cytometric plots. All assays shown represent means of at least triplicate biologic assays.

Mammosphere-formation Assay

Single cell suspensions were prepared in serum-free mammosphere medium and seeded in ultra-low attachment plates as in [Dontu et al. \(2003\)](#). Mammospheres > 75 μ m diameter were counted after 10-14 days using GelCount (Oxford Optronix). All assays shown represent means of at least triplicate biologic assays.

Western-Blotting

Westerns were performed in at least 3 different biologic repeats and representative data shown as described ([Sandhu et al., 1997](#)). Whole cell lysates were prepared using RIPA buffer (Cell Signaling) supplemented with 1X protease and phosphatase inhibitor cocktails (G-Biosciences). Usually 20 μ g protein/lane were subjected to SDS-PAGE and then transferred to a PVDF blotting membrane (Bio-Rad). The membranes were incubated with the indicated primary antibodies and HRP-conjugated secondary antibodies (Promega). The immune-reactive bands were visualized using a chemiluminescent substrate (Thermo Scientific) and X-ray film (Phenix Research Products).

In vitro Dual Luciferase Assays

MCF7 were transfected with pLenti.PGK.blast-Renilla Luciferase (pRL) plasmid, from Reuben Shaw (Addgene plasmid #74444; <http://addgene.org/74444>; RRID: Addgene_74444), a control lentiviral vector which expresses Renilla luciferase for data normalization ([Toyama et al., 2016](#)). For NF κ B luciferase assays, MCF7-pRL were also transfected with pGL4.32[luc2P/NF- κ B-RE/Hygro] vector (Promega), which contains five copies of a κ BRE response element that drives transcription of the luciferase reporter gene *luc2P*. For ERE luciferase assays, MCF7-pRL were also transfected with pGL4 [Luc2P/ERE/Hygro] vector (Promega #E6701), engineered to bear three copies of an ERE promoter, driving transcription of the luciferase reporter gene *luc2P*. Firefly and Renilla luciferase reporter activity was measured using Dual-Luciferase Reporter Assay System (Promega) per manufacturer's instructions.

Estrogen Concentration Assays

After 48 h and 6 days of mono-culture or co-culture, media were collected and estrogen concentrations assayed by ELISA kits for E2 and E1 (LifeSpan BioSciences) using a Promega Glomax Multi Detection Plate Reader (Promega). When tumors reached 1000 mm³, tumor lysate was prepared from at least 3 tumors/group and E2 and E1 concentrations assayed in our lab by ELISA (Lifespan BioSciences). For data confirmation, different triplicate sample were sent to University of Virginia (UVA) Center for Research and Reproduction Ligand Assay and Analysis Core Laboratory (Charlottesville, VA). The UVA Core laboratory used ALPCO ELISA kits for E2 assays, and E1 was assayed by radioimmunoassay. Results were highly concordant for UVA and our ELISA assays and between the ELISA and RIA data, and data shown represent the mean of all assay for each steroid.

Chromatin Immunoprecipitation Assay

For chromatin immunoprecipitation (ChIP) assays for the *CCL2* and *IL6* promoters, soluble chromatin was prepared from 2×10^7 cells as in [Nettles et al. \(2008\)](#). The chromatin solution was diluted 10-fold with ChIP dilution buffer (1.1% Triton X-100, 1.2 mM EDTA, 167 mM NaCl, 16.7 mM Tris-HCl, pH 8.1, 0.01% SDS, plus protease and phosphatase inhibitors), pre-cleared, and blocked with 2 μ g of sheared salmon sperm DNA and pre-immune serum. Pre-cleared chromatin was used in immunoprecipitation assays with anti-p65/RelA (Cell Signaling), anti-ER α (mAb F1 Cell Signaling), anti-SRC3 (Bethyl Laboratories), anti-CBP/p300 (Cell Signaling), CBP (Santa Cruz), anti-H3K27Ac (Cell Signaling), or an anti-IgG (Santa Cruz) antibody. In addition to IgG controls, all TF binding assays used unrelated promoter specific controls to show binding was specific. The washed antibody-protein-DNA complexes were eluted from the beads in 1% SDS, 0.1 M NaHCO₃ at room temperature for 20 min. 20 μ g/ μ l of proteinase K was used for removal of protein at 2 h at 55°C and reverse cross-linking was performed incubating at 65°C overnight. Purified DNA was subjected to QPCR with primers specific for the *CCL2*, *IL6*, *PS2* and *GREB1* promoter binding sites. All ChIP analyses were performed as triplicate technical repeats for each of 3 biologic repeat assays. Primer sequences including those for non-sequence specific controls are shown in [Key Resources Table](#).

Estrogen Regulation of Obesity-Mediated NF- κ B Activity In Vivo

NF- κ B-luc (B10. Cg-*H2^k* Tg(NF κ B/Fos-luc)26Rinc/J) female mice were fed with a Low Fat Diet (LFD) or a High Fat Diet (HFD) starting at the age of 21 days and then ovariectomized at week 6. For the first experiment, 0.37 mg 90 day release pellets of either E1 or E2 (Innovative Research of America) were implanted at week 6 and all control mice were implanted with control pellets without estrogen ([Figure 4A](#)). For the second experiment, 0.1 mg 90 day release pellets of either E1 or E2 were implanted at week 24, using implanted placebo pellets for control mice ([Figure 4D](#)). This mouse model expresses the luciferase gene driven by two copies of the NF κ B-RE, which allows the study of NF κ B pathway activation by IVIS. Mice were injected intraperitoneally with 10 μ L/g of body weight with a solution of Luciferin (PerkinElmer) prepared in PBS at 15 mg/mL, and bioluminescence measured after 10 min. Bioluminescence was monitored by Xenogen IVIS weekly or biweekly (Perkin Elmer) and analyzed with Living Image software (Perkin Elmer). Experiments used 10 mice/group.

Lentivirus Production and Establishment of HSD17B14 Expressing Cells

Lentivirus vectors encoding ORF HSD17B14 and ORF control were purchased from GeneCopoeia. Lentivirus vectors encoding different ORFs, were co-transfected with DeltaVPR and CMVSVG plasmids (Addgene) into asynchronous 293T with Lipofectamine

3000 Reagent. Viral supernatants were collected after 48 and 72 h. MCF7, T47D and MDA-MB-361 cells stably transduced with expression clone were incubated for 8–16 h with the medium containing the virus, supplemented with 4 $\mu\text{g}/\text{mL}$ of polybrene (Sigma-Aldrich). Cells were infected twice with polybrene, selected with 2 $\mu\text{g}/\text{mL}$ of puromycin and analyzed 3–5 days post infection by RFP visualization and overexpression was confirmed by western blotting. Cells were maintained in IMEM, RPMI or DMEM plus 10% FBS and 0.2 $\mu\text{g}/\text{mL}$ of puromycin was used to maintain the cell line.

CRISPR Mediated HSD-17B14 Knockout Lines

Transfections of MCF7 and T47D cell lines with (sc-418922) HSD17B14 CRISPR/Cas9 KO Plasmid (sc-418922) and HSD17B14 HDR plasmids was done with Ultra-Cruz Transfection Reagent (Santa Cruz, sc-395739) according to the manufacturer's instructions. Loss or of targeted proteins was confirmed by qPCR and WB.

RNA Sequencing (RNA-seq)

Total RNA quality was measured using Bioanalyzer RNA Nano 6000 (Agilent Technologies, Santa Clara, CA, USA). Library preparation was performed by NEB Next Ultra (II) Directional RNA Library Prep (Illumina, San Diego, USA), and quality confirmed using KAPA Pure Beads (Kapa Biosystems, Wilmington, MA, USA). Paired end sequencing was performed on Illumina NextSeq platform using 150 cycles 400M kit. All RNA seq experiments were performed in triplicate on independent biologic repeat assays.

Orthotopic Tumor Formation Assays

Mice were oophorectomized at day 21 and estrogen pellets implanted within 10 days with 90 day release pellets delivering 0.1 mg of either E1 or E2 (Innovative Research of America). No estrogen control mice were implanted with placebo pellets. For orthotopic xenograft assays, 5×10^5 cells from each MCF7 group were suspended in 100 μL Matrigel and injected 3 days after oophorectomy into the 4th mammary fat-pad of 5–6 week old NOD-SCID mice, using eight animals/group. Tumor growth was monitored by twice-weekly caliper measurement and volumes calculated as $(\text{long-side} \times \text{short-side}^2)/2$. Primary tumors were removed when they reached 1000 mm^3 . Primary tumors were excised, dissociated and then used for limiting dilution T-ISC quantitation assays in secondary NSG mice (see below).

A second MCF7 experiment was carried out to assay tumor growth with and without the SERD, fulvestrant ($n = 8/\text{group}$). Where indicated fulvestrant, 5mg/mouse was given once per week s.c.

For syngeneic orthotopic mammary tumor formation using the E0771 model, 1×10^4 E0771 cells were suspended in 100 μL Matrigel and then injected into the 4th mammary fat-pad of C57BL/6J mice, using 5 animals/group. For estrogen supplementation, mice were implanted with 90 days release pellets delivering 0.1 mg of either E1 or E2 (Innovative Research of America). No estrogen control mice were implanted with placebo pellets. For fulvestrant therapy, 5 mg/mouse was given s.c. once per week. Tumor growth was monitored by twice-weekly caliper measurement and volumes calculated as $(\text{long-side} \times \text{short-side}^2)/2$.

Assays with Dissociated Xenograft Tumor Cells

Primary dissociated MCF7 and MCF7HSD tumors were removed at 1000 mm^3 , dissociated into single cell suspensions and then assayed directly for ALDH1 activity by Aldefluor assay or injected into secondary recipient mice in limiting dilutions to quantitate tumor initiating stem cells (T-ISC) as in [Ginestier et al. \(2007\)](#). For limiting dilution T-ISC assays, 5 week-old female NSG mice were purchased from Jackson Labs (Boston, MA, USA). Limiting dilutions of 10000, 20000, and 60000 cells were each suspended in 10 mg/mL Matrigel with Hanks' Balanced Salt Solution (HBSS; Lonza, Walkersville, MD, USA), and injected into the 4th inguinal mammary fat pad ($n = 8$ mice per group, respectively) ([Ginestier et al., 2007](#)). For estrogen supplementation, mice were implanted with 90 day release pellets delivering 0.1 mg of either E1 or E2. No estrogen control mice were implanted with no-estrogen placebo pellets. Mice were euthanized per IACUC guidelines. Tumor size was measured twice/week, and tumor volumes were estimated as $\text{length} \times \text{width} \times \text{width} \times 0.5$. T-ISC frequency was calculated by L-Calc Limiting Dilution Software (STEMCELL). All animal work was carried out in compliance with the Institutional Animal Care and Use Committee of University of Miami.

Immunohistochemistry

Primary xenograft tumors were fixed in 10% neutral buffered formalin for 24 h and then paraffin embedded. Tumor sections were cut at 4 μm and Ki67 detected by immunohistochemistry as in [Chen et al. \(2009\)](#). For antigen retrieval, samples were immersed in sodium citrate (10 mM, pH 6.0) and microwaved for 45 min. Sections were incubated in Ki67 antibody (1:50) overnight at 4°C, followed by horseradish peroxidase (HRP)/DAB subtract complex and photomicrographs prepared as in [Simpkins et al. \(2012\)](#).

RNA-seq Bioinformatic Analysis

Quality and adaptor trimming was performed using cutadapt 1.15. Transcriptome alignment and quantification was performed using RSEM 1.3.0 and STAR 2.0.6c against human transcriptome (GRCh38_no_alt_analysis_set_GCA_000001405.15 and GENCODE v28). Differentially expressed genes were identified using DESeq2 1.18.1 with median-ratio normalization, and heatmaps, clustering and PCA plots were generated using sample blind variance stabilized log2 gene counts. To further evaluate genes identified as uniquely up or downregulated by E1 or E2 in the initial analysis, differential expression was evaluated by DESeq2 analysis after combining all E1 and E2 data together and comparing this against the cFBS group. Most genes identified as uniquely regulated by either E1 or E2 with FDR < 0.05 following the comparison of each group versus cFBS were also confirmed in the analysis of

the combined E1 and E2 data versus cFBS. Gene Set Enrichment Analysis (GSEA 3.0.1) was performed using Wald statistic ranked genes lists (Subramanian et al., 2005). Gene sets that enriched with a BH FDR < 0.05, that have the top 20 positive or negative NES scores, and that are relevant for breast cancer pathways were presented in figures. KEGG 2016 pathway enrichment was performed using Enrichr. Pathways were presented if BH FDR < 0.05, were in the top ten significant pathways, and relevant for breast cancer.

Analysis of TNF α and Estrogen Regulated Genes in Primary ER+ Human Breast Cancers

Primary human ER+ breast cancers were analyzed from The Cancer Genome Atlas (TCGA) as of 1-23-19. A subset of 255 genes upregulated by TNF α were further upregulated by addition of E1 but not by E2. Univariate Cox regression for each of the 255 genes was undertaken to determine contribution to risk in 326 ER+ breast cancers that expressed all of these genes. Candidate genes were selected one by one based on poor prognosis to 5 year disease free survival (DFS) in a univariate Cox model ($p < 0.05$). This yielded a 16 gene signature that was used to segregate patients into two groups by principal component analysis for subsequent Kaplan Meier and hazard analyses. The prognostic importance of this 16 gene signature was then validated versus overall survival in 722 ER+ breast cancers from the METABRIC dataset (1-10-19).

QUANTIFICATION AND STATISTICAL ANALYSIS

All graphed data are presented as mean \pm SEM from at least 3 biological replicate experiments done in triplicate technical repeats. Student's t test was used for experiments with two groups. Comparisons of > 2 groups used one-way analysis of variance (ANOVA) followed by Dunnett's or Tukey's post hoc analysis. Some experiments used two-way analysis of variance followed by Tukey's post hoc tests. Statistical significance values were set as * $p < 0.05$. ** $p < 0.01$. *** $p < 0.001$. A p value less than 0.05 would be considered statistically significant, ns = not significant. p value and n can be found in main and supplementary figure legends. Statistical differences between tumor growth curves used 'Compare Growth Curves' function statmod software package (<http://bioinf.wehi.edu.au/software/compareCurves/>). UALCAN <http://ualcan.path.uab.edu/index.html> was used to study expression of HSD17B14 in primary breast cancers and normal breast tissues from the TCGA database. For analysis of differences in the HSD17B14 expression in primary breast cancers and normal breast tissues, t test was performed using a PERL script with Comprehensive Perl ArchiveNetwork (CPAN) module "Statistics::TTest" (<http://search.cpan.org/~yunfang/Statistics-TTest-1.1.0/TTest.pm>).